NTNU – Trondheim
Norwegian University of
Science and Technology

Analysis and Simulation of the Rate of Heat Release (ROHR) in Diesel Engines

Raimon Andreas Olsen

Marine Technology (2 year)
Submission date: June 2013
Supervisor: Harald Valland, IMT

Norwegian University of Science and Technology
Department of Marine Technology

NTNU
The Norwegian University of Science and Technology

Faculty of Engineering Science and Technology
Department of Marine Technology

MSc-ASSIGNMENT
for
Stud.techn. Raimon Andreas Olsen

Spring semester 2013

Analysis and simulation of Rate of Heat Release (ROHR) in diesel engines

Analyse og simulering av energiomsetningshastigheten (ROHR) i dieselmotorer.

Overall Aim and Focus

The project assignment should study the combustion properties of fuels expressed by ROHR, thermal efficiency, fuel consumption, exhaust emissions (except particles) for several types of renewable diesel fuels by experiments using the Hydra Diesel engine.
A part of the project will deal with the Hydra Diesel, its data monitoring system, analysis of measurements, and report generation. Methods and algorithms developed should be independent of a particular engine type.

The assignment should be prepared based on following points:

- Analysis of the combustion process based on measurement of dynamic cylinder pressure. Special emphasis should be put on computation and analysis of Rate of Heat Release ROHR and total heat release THR.
- Methods should be developed for determining crank angle at ignition, ignition delay and main characteristics of the heat release pattern such as combustion duration.
- The rate of heat release may de approximated by one or more Viebe functions. Methods for determining the corresponding Viebe-coefficients should be considered.
- Assessment of using ROHR as a metric in engine testing of fuels.

The assignment text must be included as a part of the project report.

The report should be written like a research report, with an abstract, conclusions, contents list, reference list, etc. During preparation of the report it is important that the candidate emphasizes easily understood and well written text. For ease of reading the report should contain adequate references at appropriate places to related text, tables and figures. On evaluation, a lot of weight is put on thorough preparation of results, their clear presentation in the form of tables and/or graphs, and on comprehensive discussion.
All used sources must be completely documented. For textbooks and periodicals, author, title, year, page number and eventually figure number must be specified.

In accordance with current regulations NTNU reserves the right to use any results from the project work in connection with teaching, research, publication, or other activities.

The project report must be delivered no later than June 10, 2013.

Department of Marine Technology, 2013-01-14

Harald Valland
professor

Abstract

Analysis and Simulation of the Rate of Heat Release (ROHR) in Diesel Engines

by Raimon Andreas Olsen

As the restrictions for emissions from diesel engines are getting stricter, alternative fuels get more attention. Alternative fuels that can be used directly on already existing engines must be investigated to compare their performance with conventional fuels. When analyzing the combustion process in engines it is necessary to take into consideration that the working medium changes both its composition and its thermodynamic properties under combustion. This way the analysis of the in-cylinder process becomes more accurate. Using the First Law of Thermodynamics as a foundation two simulation models are constructed for the calculation of several in-cylinder engine parameters. The models were tested with measurements done on a test engine and several outputs were presented. The test working points were based on the generator and propeller loading curve, which gave 8 measured cylinder pressure traces.

Calculation of the speed of combustion (reaction rate) from the pressure measurements gave useful results and the performance of the test engine was calculated based on these. Integration of the reaction rates give the reaction co-ordinates (RCOs), which tells how much fuel that is burned at any time. The calculated RCOs in this case gave results that were partly impossible and the reasons for this were sought. This gave indications that errors in the pressure measurement could be the cause of this.

Small fluctuations in the pressure measurements will cause big fluctuations in the calculated reaction rate and thus rate of heat release (ROHR). The reaction rate from raw measurements can be smoothed by the aid of Vibe functions. A smoothing attempt was carried out, but the results were rather poor. The impact of the Vibe parameters is demonstrated. The developed models show results that indicate a good validity.

Sammendrag

Analyse og Simulering av Energiomsetningshastigheten (ROHR) i Dieselmotorer

av Raimon Andreas Olsen

Strengere krav til utslipp fra dieselmotorer gjør at alternative drivstoff får mer oppmerksomhet. Alternative drivstoff som kan bli brukt på allerede eksisterende dieselmotorer må undersøkes for å sammenligne deres ytelse og anvendelighet relativt konvensjonell diesel. For at en analyse av sylinderprossesen i en dieselmoter skal være rkitigst mulig, er det nødvendig å ta hensyn til at arbeidsmediet endrer sammensetning og at de termodynamiske egenskapene endres. To modeller er utviklet på grunnlag av termodynamikkens første lov for å kunne beregne/simulere hva som skjer i kompresjons, forbrennings og ekspansjonsfasen i en dieselmoter. Gjennom å ta 8 trykkmålinger på en testmotor, kunne modellene testes og resultater for denne motoren bli presentert.

Resultatene for forbrenningshastighen (reaksjonshastigheten) beregnet fra det målte trykkforløpet var gode, og motorens ytelse ble beregnet utfra dette. Integrasjon av forbrenningshastigheten vil gi mengde drivstoff som er forbrent etter en bestemt tid i forbrenningsprossesen. Da denne størrelsen ble beregnet ga den på visse steder verdier som var umulige. Årsakene til dette ble forsøkt funnet. Dette indikerte at det målte trykket kan være noe feil.

Forstyrrelser i trykkmålingene vil føre til store forstyrrelser i det beregnede forbrenningshastighetssignalet og dermed energiomsetningshastigheten. Det er mulig å glatte disse forstyrrelsene ved hjelp av såkalte Vibe-funksjoner. Et forsøk på glatting av målingene fra test motoren førte til heller dårlige resultater. Dette på grunn av manglende tid og erfaring med den spesifikke programvaren. Effekten av å variere på de ulike parametrene som inngår i en Vibe-funksjon er vist. De utviklede modellene viser fornuftige resultater.

Acknowledgements

I would like to thank my supervisor Prof. H. Valland for being available and answering questions that came up during the work, as well as being a source of motivation.

Great thanks go to Prof. D. Stapersma at Deflt University of Technology who gave necessary help in the modeling phases of the work.

Thanks to my two fellow students Mika and Paal for great aid in the use of MATLAB/Simulink, and for valuable non-school related recreation.

Laboratory engineer Frode Gran was helpful in the laboratory tests.

Lastly I would like to thank my family, who always supports and believes in me.

Contents

List of Figures

List of Tables

Abbreviations

ABDC	**A**fter **B**ottom **D**ead **C**enter
BTDC	**B**efore **T**op **D**ead **C**enter
CRR	**C**ombustion **R**eaction **R**ate
da	**d**ry **a**ir
EOC	**E**nd **O**f **C**ombustion
EO	**E**xhaust **O**pens
GTL	**G**as **T**o **L**iquid
GAHRR	**G**ross **A**pparent **H**eat **R**elease **R**ate
IC	**I**nlet **C**loses
IMO	**I**nternational **M**aritime **O**rganization
LHV	**L**ower **H**eating **V**alue
LNG	**L**iquefied **N**atural **G**as
NAHRR	**N**et **A**pparent **H**eat **R**elease **R**ate
ROHR	**R**ate **o**f **H**eat **R**elease
RCO	**R**eaction **C**o- **O**rdinate
SOC	**S**tart **O**f **C**ombustion
SECA	**S**ulfur **E**mission **C**ontrol **A**reas
sg	**s**toichiometric **g**as
UHC	**U**nburned **H**ydro **C**arbons

Symbols

A	area	[m^2]
a	vibe parameter	[-]
a_k	power series coefficient	[-]
b_1	vibe weighting factor	[-]
b_2	vibe weighting factor	[-]
C_k	constants in woschni equation	[m/s K]
c_m	mean piston speed	[m/s]
C_v	specific heat capacity at constant volume	[kJ/kgK]
C_p	specific heat capacity at constant pressure	[kJ/kgK]
CR	ratio of crank radius and connecting rod	[-]
D	diameter	[m] [mm]
e_f	specific energy of liquid fuel	[kJ/kg]
$\dot{E}$	energy flow	[kW]
h	specific enthalpy	[kJ/kg]
k	proportionality constant	[-]
L_p	distance from cylinder top to piston head	[m] [mm]
L	length	[m] [mm]
m_1	vibe form factor	[-]
m_2	vibe form factor	[-]
m	mass	[kg] [g]
M_j	molar mass of constituent j	[g/mol]
mr_j	mass ratio of constituent j and 1 kg fuel	[-]
N	engine speed	[rpm]

n	engine speed	[rps]
p	pressure	[bar]
$\dot{Q}$	heat flow	[kW]
R	gas constant	[kJ/kg]
r	radius	[m] [mm]
T	temperature	[K] [°C]
t	time	[s]
u	specific internal energy	[kJ/kg]
u_{comb}	heat of combustion	[kJ/kg]
V	volume	[m^3] [liter]
$\dot{W}$	power	[kW]
w_t	swirl velocity	[m/s]
X	normalized reaction co-ordinate	[-]
x	in cylinder air fraction	[-]
x_j	mass fraction of constituent j	[-]
y_j	molar fraction of constituent j	[-]
Z	normalized reaction rate	[-]

α	heat transfer coefficient	[W/K m^2]
ε	compression ration	[-]
η	efficiency	[-]
θ	normalized temperature	[-]
λ	air excess ratio	[-]
μ	proportionality constant	[-]
ξ	reaction rate	[kg/s]
ρ	density	[kg/m^3]
σ	stoichiometric air/fuel ratio	[-]
τ	normalized time	[-]
ϕ	crank angle	°

Chapter 1

Introduction

1.1 Background and Motivation

Emissions from diesel engines are a matter of increasing attention as the regulations are getting stricter. In the consideration of emissions it is important to have some knowledge about not only the environmental concerns of each emission, but also their origin. While CO_2 and SO_2 in the exhaust from engines are almost completely determined by the fuel composition, the emissions of NO_x, unburned hydrocarbons (UHC) and CO are dependent on the in-cylinder process. Some typical emission quantities for combustion of petroleum diesel are shown in Table 1.1. Of the in-cylinder process dependent emissions NO_x is dominating.

Figure 1.1 shows the IMO limits for sulfur fractions allowed in a fuel on a global basis and for sulfur emission control areas (SECA). Already in 2015 the limits are approaching zero for SECA. This will especially influence the marine sector, which to a great extent is fueled on heavy fuel oil that contains about 3 % sulfur.

TABLE 1.1: Amounts of emissions from combustion of petroleum diesel [Stapersma, 2010a]

CO_2	SO_2	NO_x	UHC	CO	
3200	20	40 - 100	0.5 - 4	2 - 20	[g/kg_{fuel}]

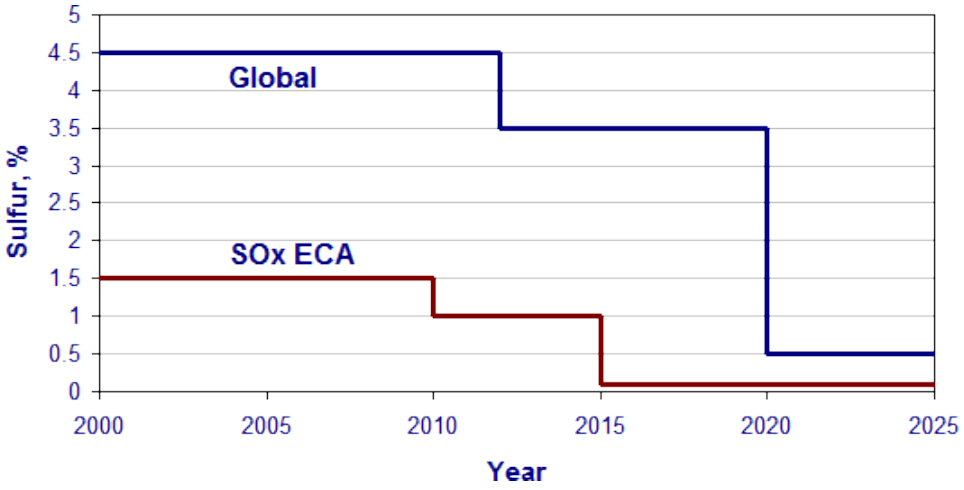

FIGURE 1.1: IMO legislations for SO_x emissions globally and in sulphur emission control areas (SECA)

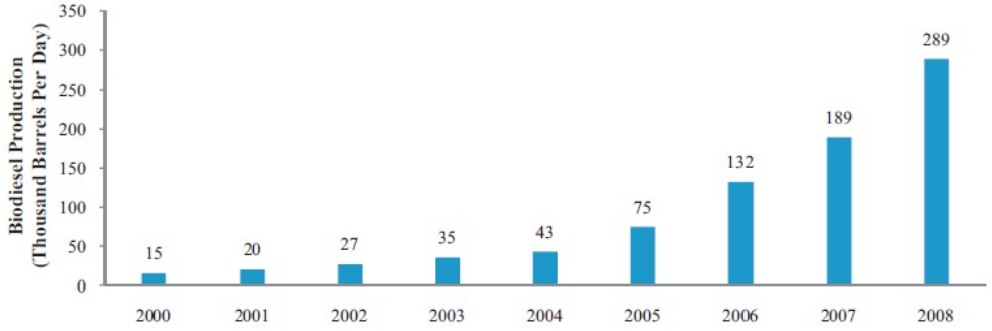

FIGURE 1.2: Total production trend of biodiesel [Atabani et al., 2012]

In the search for alternative fuels both biodiesel and liquefied natural gas (LNG) are options that have shown good results with respect to emissions. As shown in Figure 1.2 the total production trend of biodiesel over the last years has increased and is expected to do so even more. Clearly there is a connection between the increasing production of biodiesel and the more stringent emission restrictions. Opposed to for instance LNG, biodiesel can be used directly on diesel engines, which should be considered an advantage. The disadvantage of biodiesel is the high production costs which make the final product expensive. Apart from these factors biodiesel has performance parameters that are comparable to conventional diesel, and thus methods for investigating types of biodiesel and other alternative fuels more thoroughly are desired.

Statoil has donated a Ricardo Hydra test engine to the Marine Machinery Laboratory at the department of Marine Technology at NTNU in Trondheim. Their wish was to have several types of renewable fuels tested on this engine. Among the available fuels for testing are so-called GTL (gas to liquid) and fish oil. In the consideration of the suitability for usage of such fuels it is necessary with detailed information about what is going on inside the cylinder when the fuel burns. The more detailed the description of the in-cylinder process in an engine, the more reliable the comparison of the different fuels will be.

1.2 Overall Aim and Focus

Aiming for reliable and valid characterization of the in-cylinder process in a diesel engine, a method for calculating among other things the speed of the combustion reaction, the amount of fuel burned at any time in the combustion process, the rate of heat release, the heat lost to the cylinder walls, the in-cylinder gas states and the thermodynamic in-cylinder gas properties will be presented in this thesis.

Using the simulation environment MATLAB/Simulink two models based on the work of Stapersma [2010b] and Ding [2011] will be built. The first model will use an input signal of a combustion reaction speed and output the in-cylinder pressure. The second model is the reversed of the first and therefore will take a measured pressure as input and give the speed of the reaction as output. By measuring the pressure and crank angle at the Hydra test engine in the Machine Laboratory the models can be tested with real life quantities and the performance of the engine can be calculated.

The validity of the models can be checked by backwards calculation. This will be done by giving the output of the first model as input to the second. If the output of the second model equals the input of the first, it is an indication of valid models. The output from the models will also be judged for their actual physical sense, and causes of possibly unphysical results will be sought. The fundamental

equations behind the models are derived from the First Law Of Thermodynamics, and will be explained in Chapter 2. Tests on the Hydra engine will be executed after standards which will be presented in Chapter 3 together with the simulation models. Results will be presented in Chapter 4.

Initially the plan for the thesis was to test several fuel qualities on the hydra engine, but severe problems with the engine hindered this.

Chapter 2

Theoretic Fundamentals

2.1 Engine Cylinder Energy Flows

When analyzing thermodynamic systems it is necessary to define a control volume. For the diesel engine the control volume is constrained by the cylinder dimensions. The approach in this thesis is based on a single-zone combustion model as presented in Stapersma [2010b]. This means that the dwelling time of the fuel droplets and fuel gas after evaporation are both assumed to be zero. Starting with the energy and mass balance for an open control volume, it is shown that the change of temperature can be expressed as presented in (2.1), which integrated gives the temperature in the control volume. The full derivation can be found in Appendix A.

$$\frac{dT}{dt} = \frac{\dot{Q}_{comb} - \dot{Q}_{loss} - p \cdot \frac{dV}{dt} + \dot{E}_f}{m \cdot C_v} \tag{2.1}$$

Here $\dot{Q}_{comb}$ is the rate of heat release (ROHR) or combustion heat flow, $\dot{Q}_{loss}$ is the heat loss from the gas to the surrounding walls, $p\frac{dV}{dt}$ is the indicated work, $\dot{E}$ is the energy of the liquid fuel entering the cylinder, m is the in-cylinder mass and C_v the specific heat capacity at constant volume for the in-cylinder gas mixture.

2.2 Heat Release

The expression for the change of temperature can be rearranged and the gross apparent heat release rate (GAHRR) can be defined as shown in (2.2) [Stapersma, 2010b], which tells how fast the heat from combustion is released. Opposed to the net apparent heat release rate (NAHRR), the GAHRR also includes the heat loss.

$$GAHRR = \dot{Q}_{comb} + \dot{E}_f = m \cdot C_v \frac{\mathrm{d}T}{\mathrm{d}t} + \dot{Q}_{loss} + p \cdot \frac{\mathrm{d}V}{\mathrm{d}t} [kW] \tag{2.2}$$

If the GAHRR is divided by the specific energy content of the fuel, the result is the combustion reaction rate (CRR) as shown in (2.3) [Stapersma, 2010b]. The specific energy of the fuel is here the specific heat of combustion u_{comb} plus the specific energy e_f of the fuel entering in its liquid phase. Instead of expressing how fast the energy from combustion is released, the CRR tells how fast the fuel is burned.

$$CRR = \frac{m \cdot C_v \frac{\mathrm{d}T}{\mathrm{d}t} + \dot{Q}_{loss} + p \cdot \frac{\mathrm{d}V}{\mathrm{d}t}}{u_{comb} + e_f} [kg/s] \tag{2.3}$$

The expressions (2.1) and (2.3) are the basis of the two simulation models that were built and which will be presented in section 3.1.

2.3 Speed of Combustion

2.3.1 Reaction Rate

According to Stapersma [2010b] the first principle of chain reactions says that the formation of radicals $\frac{dm_f^+}{dt}$ is proportional to the amount of fuel m_f and the increase of radicals dm_f^+ is proportional to the decrease of fuel dm_f as shown in (2.4) and (2.5), respectively.

$$\frac{\mathrm{d}m_f^+}{\mathrm{d}t} = k \cdot m_f \tag{2.4}$$

$$\mathrm{d}m_f^+ = -\mu \cdot \mathrm{d}m_f \tag{2.5}$$

The speed of reaction can then be expressed as shown in (2.6). Combustion is fuel and oxygen reacting, which in this case means that $\xi = CRR$.

$$\xi = \frac{\mathrm{d}m_f}{\mathrm{d}t} = -\frac{k}{\mu} m_f \tag{2.6}$$

The integral of the reaction rate is referred to as the reaction co-ordinate (RCO), and it is the amount of fuel burned at time t as shown in (2.7).

$$RCO = \int_{t_1}^{t_2} \xi \mathrm{d}t \tag{2.7}$$

2.3.2 Vibe Functions

A CRR signal can be constructed from so-called Vibe functions, where a multiple of parameters will decide the shape of the functions. The RCO and CRR can be expressed as the normalized quantities X and Z, respectively. By assuming a non-linear time dependency for the reaction constant $\frac{k}{\mu}$, X and Z can be constructed according to (2.8) and (2.9), which show double Vibe functions.

$$X = b_1 \left(1 - e^{-a\tau^{m_1+1}}\right) + b_2 \left(1 - e^{-a\tau^{m_2+1}}\right) \tag{2.8}$$

$$Z = \frac{\mathrm{d}X}{\mathrm{d}\tau} = b_1 a \left(m_1 + 1\right) \tau^{m_1} e^{-a\tau^{m_1+1}} + b_2 a \left(m_2 + 1\right) \tau^{m_2} e^{-a\tau^{m_2+1}} \tag{2.9}$$

Where τ is the normalized time, b the weighting factors, m the form factors and a is tied to the combustion efficiency. All the coefficients can be chosen to obtain the desirable shapes of the Vibe functions. With the Vibe parameters shown in Table 2.1, X and Z will have the shapes shown in Figure 2.1.

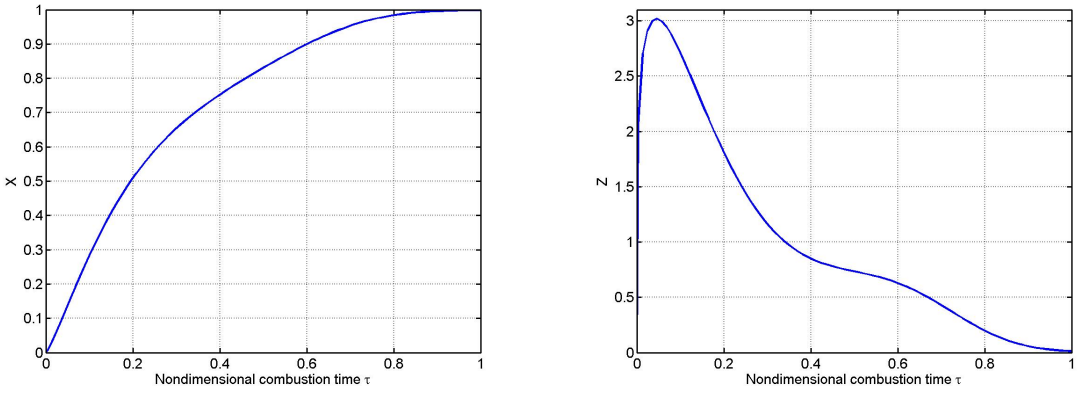

(a) Nondimensional reaction co-ordinate

(b) Nondimensional reaction rate

FIGURE 2.1: Nondimensional double Vibe functions

TABLE 2.1: Example of Vibe parameter values

Coefficient	Value
m_1	0.2
m_2	3.0
b_1	0.8
a	6.9078

It is now possible to construct a reaction rate ξ from the normalized reaction rate Z. With the total fuel available for combustion m_f^{comb} and combustion duration time Δt_{comb} according to Stapersma [2010b] the reaction rate can be expressed as shown in (2.10).

$$\xi = Z \cdot \frac{m_f^{comb}}{\Delta t_{comb}} \tag{2.10}$$

According to Ding [2011] m_f^{comb} can be found from (2.11).

$$m_f^{comb} = \frac{m_1 x_1}{\lambda \sigma_{da}} \tag{2.11}$$

Subscript $_1$ refers to the start of the compression stroke which is when the inlet valve closes, and will be referred to as the inlet closes (IC) condition. m_1 and x_1

is therefore the trapped mass and the air fraction at IC, respectively. λ is the air excess ratio and σ_{da} the stoichiometric air/fuel ratio for dry air. The trapped mass can be found by applying the gas law at IC. It is then necessary to know p_1, R_1, V_1 and T_1. These can be measured on the engine test bed if possible, or they can be assumed based on experience. Then m_1 can be found from the gas law as shown in (2.12).

$$m_1 = \frac{p_1 V_1}{R_1 T_1} \tag{2.12}$$

The duration of combustion is given by the start of combustion (SOC) and the end of combustion (EOC) in crank angle degrees, and can easily be translated to time as shown in (2.13).

$$\Delta t_{comb} = (t_{EOC} - t_{SOC})[s] = (EOC - SOC)\,[^\circ] \cdot \frac{60[s/min]}{N[rev/min] \cdot 360[^\circ/rev]} \tag{2.13}$$

Where N is the engine speed. The integral of N gives the crank angle. The stoichiometric air/fuel ratio for dry air can be calculated according to (2.14) [Stapersma, 2010b].

$$\sigma_{da} = \frac{M_{da}}{y_{O_2}} \cdot \left(\frac{x_c}{M_c} + \frac{1}{4} \cdot \frac{x_h}{M_h} + \frac{x_s}{M_s} \right) \tag{2.14}$$

Where y_{O_2} is the molar fraction of oxygen in dry air and has the value of approximately 0.21. With known fuel composition the ratio of mass fraction x and molar mass M for respectively carbon, hydrogen and sulfur can be found. The air excess ratio λ is for diesel engines usually in the range of 2 - 2.5.

2.4 Phases of Combustion

In the analysis of combustion in the diesel engine four phases are usually defined. These are the ignition delay phase, the premixed combustion phase, the diffusive combustion phase and the late burning phase.

The ignition delay period is identified by negative a ROHR, and this is due to evaporation of the fuel. The fuel needs to evaporate before it can ignite, and hence it consumes heat instead of releasing it. When satisfactory evaporation is obtained the fuel ignites, and this can be seen by a steep increase for the ROHR. The ROHR then decrease before it increases again because fuel injection persisted while the ignition and its following pressure rise occurred. This is referred to as diffusive the combustion phase. In the late combustion phase the ROHR is decreasing till it reaches zero.

2.5 Heat of Combustion

The ROHR can be found by multiplying the CRR with the heat of combustion u_{comb} as shown in (2.15).

$$\dot{Q}_{comb}[\text{kW}] = CRR[\text{kg/s}] \cdot u_{comb}[\text{kJ/kg}] \tag{2.15}$$

In most studies the heat of combustion is considered to be a constant value. For diesel typically an LHV value around 43-44 [MJ/kg] is used. However, this is not completely correct since the actual value will vary with the temperature. According to Ding [2011] the heat of combustion can be calculated from (2.16).

$$u_{comb} = u_f + \sigma_{da} \cdot u_{da} - (1 + \sigma_{da}) \cdot u_{sg} \tag{2.16}$$

Where u_f, u_{da} and u_{sg} are the specific internal energies for respectively fuel, dry

air and stoichiometric gas. These can be calculated from temperature power series expansions, and the procedure will be explained in section 2.6.

2.6 In-Cylinder Working Medium

2.6.1 Thermodynamic Properties

To be able to calculate the energy content for the in-cylinder gas at any time, it is necessary to establish specific heat capacities, specific internal energies and specific enthalpies that are functions of temperature and composition. At the SOC the in-cylinder gas is assumed to be air while at the end of combustion (EOC) it will be a mixture of air and stoichiometric gas. The composition of dry air is well established, and the composition of stoichiometric gas can be calculated when the fuel type is known. The temperature dependency will be established on the basis of power series given in Stapersma [2010c] and Ding [2011].

The power series expansions are normalized and therefore the temperature needs to be normalized as shown in (2.17). Here T_{norm} =1000 [K].

$$\theta = \frac{T}{T_{norm}} \tag{2.17}$$

With the normalized temperature the specific heat at constant pressure for the different constituents j can be found from (2.18)[Stapersma, 2010c].

$$C_{p,j} = R_j \sum_{k=1}^{m} a_{k,j} \cdot \theta^{k-1} \left[\frac{\text{kJ}}{\text{kg K}}\right] \tag{2.18}$$

Where the power coefficients a_k can be found in Appendix B Table B.1. The gas constant R_j can be found from (2.19).

$$R_j = \frac{R_u}{M_j} \tag{2.19}$$

Where R_u is the universal gas constant equal to 8.3144621 [J/mol K], and M_j the respective molar mass.

Knowing the mass fractions of constituents x_j of dry air (da) and stoichiometric gas (sg), a summation can be done as shown in (2.20) and (2.21).

$$C_p^{da} = \sum_j x_j^{da} \cdot C_{p.j} \tag{2.20}$$

$$C_p^{sg} = \sum_j x_j^{sg} \cdot C_{p.j} \tag{2.21}$$

The specific heat capacity at constant volume C_v for the in-cylinder gas can then be calculated as shown in (2.22) and (2.23).

$$C_v^{da} = C_p^{da} - R^{da} \tag{2.22}$$

$$C_v^{sg} = C_p^{sg} - R^{sg} \tag{2.23}$$

The specific internal energies and specific enthalpies are by definition given as shown in (2.24) and (2.25).

$$\begin{aligned} \mathrm{d}u &= C_v \mathrm{d}T \\ u - u_{ref} &= \int_{T_{ref}}^{T} C_v \mathrm{d}T \end{aligned} \tag{2.24}$$

$$\begin{aligned} \mathrm{d}h &= C_p \mathrm{d}T \\ h - h_{ref} &= \int_{T_{ref}}^{T} C_p \mathrm{d}T \end{aligned} \tag{2.25}$$

Since the specific heat capacities are given by the power series expansions, the integration can be done for each constituent as shown in (2.26) and (2.27).

TABLE 2.2: Mass fractions of constituents in dry air[Stapersma, 2010b]

Constituent	Mass fraction
N_2	0.7553
O_2	0.2315
Ar	0.0128
CO_2	0.0005

$$h_j - h_{j,ref} = \sum_{k=1}^{m} \frac{a_{k,j}}{k} \cdot T_{norm} \cdot \theta^k - \sum_{k=1}^{m} \frac{a_{k,j}}{k} \cdot T_{norm} \cdot \theta_{ref}^k \tag{2.26}$$

$$u_j - u_{j,ref} = h_j - R_j \cdot T \tag{2.27}$$

The reference enthalpy for each species can be found in Appendix B Table B.2. The constituents of dry air is assumed to be N_2, O_2, Ar and CO_2, and the mass fractions used are shown in Table 2.2.

The specific internal energies and enthalpies for dry air and stoichiometric gas can then be found by summation of the constituents as shown in (2.28) and (2.29), respectively.

$$\begin{aligned} u^{da} &= \sum_j x_j^{da} \cdot u_j^{da} \\ u^{sg} &= \sum_j x_j^{sg} \cdot u_j^{sg} \end{aligned} \tag{2.28}$$

$$\begin{aligned} h^{da} &= \sum_j x_j^{da} \cdot h_j^{da} \\ h^{sg} &= \sum_j x_j^{sg} \cdot h_j^{sg} \end{aligned} \tag{2.29}$$

The constituents of stoichiometric gas will depend on what fuel is being used, and the composition calculation procedure will be explained in section 2.6.2. The

properties of the fuel itself can be determined in a similar manner as explained for the cylinder gas, and the details will be presented in section 2.6.3.The calculation procedure for the in-cylinder air fraction x will be explained in section 2.6.4. Eventually it is possible to establish the properties that changes with both temperature and composition as shown in (2.30),(2.31) and (2.32).

$$C_v(T,x) = x \cdot C_v^{da} + (1-x) \cdot C_v^{sg} \tag{2.30}$$

$$u(T,x) = x \cdot u^{da} + (1-x) \cdot u^{sg} \tag{2.31}$$

$$h(T,x) = x \cdot h^{da} + (1-x) \cdot h^{sg} \tag{2.32}$$

2.6.2 Stoichiometric Gas Composition

It is possible to calculate the mass fractions in the produced stoichiometric gas from the known fuel fractions, air fractions and molar masses by looking at the mass balances. The equations (2.33) - (2.38) [Stapersma, 2010b] expresses the mass of each constituent compared to 1 [kg] of fuel (mr_j). These equations calculate the reaction end products. If there is an air excess, there will be oxygen in the reaction products. Setting λ to 1 makes the reaction end products equal to stoichiometric gas.

Nitrogen

$$mr_{N_2} = y_{N_2}^{da} \cdot \frac{M_{N_2}}{M_{da}} \cdot \lambda \cdot \sigma_{da} \tag{2.33}$$

Oxygen

$$mr_{O_2} = y_{O_2}^{da} \cdot \frac{M_{O_2}}{M_{da}} \cdot (\lambda - 1) \cdot \sigma_{da} \tag{2.34}$$

Argon

$$mr_{Ar} = y_{Ar}^{da} \cdot \frac{M_{Ar}}{M_{da}} \cdot \lambda \cdot \sigma_{da} \tag{2.35}$$

Carbon-Dioxide

$$mr_{CO_2} = \frac{M_{CO_2}}{M_C} \cdot x_c \tag{2.36}$$

Sulfur-Dioxide

$$mr_{SO_2} = \frac{M_{SO_2}}{M_S} \cdot x_s \tag{2.37}$$

Water

$$mr_{H_2O} = x_{H_2O} \cdot \lambda \cdot \sigma_{da} + \frac{1}{2} \frac{M_{H_2O}}{M_H} \cdot x_h \tag{2.38}$$

Thus the mass fractions in the stoichiometric gas can be found according to (2.39).

$$x_j = \frac{mr_j}{\sum mr_j} \tag{2.39}$$

2.6.3 Fuel Specification

Gaseous Fuel

The properties for the fuel in the gaseous state are obtained by assuming that it consists of an alkane ($C_{13}H_{28}$) and a benzene (aromatic) ($C_{13}H_{10}$). From the power series presented in section 2.6.1 and the respective coefficients from Table B.1, the thermodynamic properties for the gaseous fuel can be calculated. The mass fractions of alkane and benzene can be calculated from the known composition of carbon and hydrogen in the fuel. Assuming that the fuel mass fractions

are respectively x_C, x_H, x_S, x_O and x_N, the part of the fuel consisting of carbon and hydrogen can be expressed in terms of mass fractions of the alkane (alk) and benzene (aro) as shown in (2.40).

$$x_{alk} + x_{aro} = x_C + x_H \tag{2.40}$$

The mass fractions of carbon and hydrogen can be expressed separately as shown in (2.41) and (2.42).

$$x_C = \frac{13M_C}{M_{alk}} x_{alk} + \frac{13M_C}{M_{aro}} x_{aro} \tag{2.41}$$

$$x_H = \frac{28M_H}{M_{alk}} x_{alk} + \frac{10M_H}{M_{aro}} x_{aro} \tag{2.42}$$

Where M are the respective molar masses. The two equations can be solved for the two unknowns and eventually the mass fractions of alkene and aromat can be expressed as shown in (2.43) and (2.44).

$$x_{alk} = \frac{x_C - \frac{13M_C}{M_{aro}} (x_C + x_H)}{\frac{13M_C}{M_{alk}} - \frac{13M_C}{M_{aro}}} \tag{2.43}$$

$$x_{aro} = x_C + x_H - x_{alk} \tag{2.44}$$

Then the properties of the fuel can be expressed as shown in (2.45), (2.46) and (2.47).

$$C_{v,f} = \frac{C_{v,aro} \cdot x_{aro} + C_{v,alk} \cdot x_{alk}}{x_{alk} + x_{aro}} \tag{2.45}$$

$$u_f = \frac{u_{aro} \cdot x_{aro} + u_{alk} \cdot x_{alk}}{x_{alk} + x_{aro}} \tag{2.46}$$

$$h_f = \frac{h_{aro} \cdot x_{aro} + h_{alk} \cdot x_{alk}}{x_{alk} + x_{aro}} \tag{2.47}$$

With $C_{v,aro}$, $C_{v,alk}$, u_{aro}, u_{alk}, h_{aro} and h_{alk} being calculated from the method presented in section 2.6.1. The reference enthalpy for the fuel was calculated by

comparing the lower heating value (LHV) with the heat of combustion at a reference temperature of 25 °C. The difference between u_{comb} and the LHV at the reference temperature is the reference enthalpy for the fuel, and was calculated as shown in (2.48).

$$h_f^{ref} = LHV - \sigma_{da} \cdot h^{da}_{@25\,^\circ\mathrm{C}} - (1 + \sigma_{da}) \cdot h^{sg}_{@25\,^\circ\mathrm{C}} + h^{evap}_{f@25\,^\circ\mathrm{C}} \tag{2.48}$$

Where the enthalpies of respectively dry air, stoichiometric gas and the evaporation enthalpy at 25 °C are used. The evaporation reference enthalpy was calculated from (2.49).

$$h^{evap}_{f@25\,^\circ\mathrm{C}} = \frac{h^{evap}_{aro,ref} \cdot x_{aro} + h^{evap}_{alk,ref} \cdot x_{alk}}{x_{aro} + x_{alk}} \tag{2.49}$$

Where the evaporation reference enthalpies for the aromat and alkene can be found in Appendix B Table B.3. The LHV was calculated from the formula shown in (2.50) [Stapersma, 2010b].

$$LHV = \left(46932 - \frac{8792\left(\rho_f^{15}\right)^2}{1000000}\right)(1 - x_{H_2O} - x_s) + 9420x_s - 2499x_{H_2O}\ \text{[kJ/kg]} \tag{2.50}$$

Where ρ_f^{15} is the density at 15 °C, and x_j the respective mass fractions in the fuel.

Liquid Fuel

The liquid fuel properties are different from the gaseous ones. The enthalpy of the liquid fuel was calculated as shown in (2.51) [Ding, 2011].

$$h_{f,liq} = u_{f,liq} + \frac{p}{\rho_{f,liq}}$$

$$h_{f,liq} = u_{f,ref} + C_{v,f,liq} \cdot (T - T_{ref}) + \frac{p}{\rho_{f,liq}} \tag{2.51}$$

$$h_{f,liq} = h_{f,ref} - \frac{p_{ref}}{\rho_{f,ref}} + C_{v,f,liq} \cdot (T - T_{ref}) + \frac{p}{\rho_{f,liq}}$$

Where the density of a liquid can be calculated according to (2.52) [Stapersma, 2010b].

$$\rho_{f,liq} = \rho_{f,liq}^{15} - 0.68 \cdot (T - 15) \tag{2.52}$$

Where T is the temperature in °C.

$C_{v,f,liq}$ was found from (2.53), where $C_{v,aro,liq}$=2.21 [kJ/kgK] and $C_{v,alk,liq}$=1.7 [kJ/kgK] [Ding, 2011].

$$C_{v,f,liq} = \frac{C_{v,aro,liq} \cdot x_{aro} + C_{v,alk,liq} \cdot x_{alk}}{x_{aro} + x_{alk}} \tag{2.53}$$

It is assumed that the fuel enters the cylinder at a temperature of 40 °C.

According to Ding [2011] the energy of the fuel $\dot{E}$ can then be expressed as shown in (2.54).

$$\dot{E}_f = \xi \cdot (h_{f,liq} - u_f) \tag{2.54}$$

2.6.4 Mass and Air Fraction

The in-cylinder mass will be almost constant, but increases a little bit due to the injection of fuel. If the reaction rate is integrated from IC to EO, it will give the mass addition. The total mass in the cylinder will be the trapped mass m_1 plus the RCO as shown in (2.55) [Ding, 2011].

$$m = m_1 + \int_{t_{IC}}^{t_{EO}} \xi \, \mathrm{d}t \tag{2.55}$$

Accordingly the air fraction x can be calculated as shown in (2.56) [Ding, 2011]. The air fraction is used to calculate the changing specific heat capacities explained in section 2.6.1.

$$x = \frac{m_1 x_1 - \sigma_{da} \cdot \int_{t_{IC}}^{t_{EO}} \xi \, \mathrm{d}t}{m_1 + \int_{t_{IC}}^{t_{EO}} \xi \, \mathrm{d}t} \tag{2.56}$$

2.7 Cylinder Volume

In order to obtain the dynamic cylinder volume and its time derivate the expression for the distance from the top of the cylinder to the piston is needed. This distance is a function of the crank angle ϕ as shown in (2.57).

$$L_p(\phi) = L_s \left(\frac{1}{\varepsilon - 1} + \frac{1}{2} \left(1 - \cos\phi + \frac{1}{CR} \left(1 - \sqrt{1 - CR^2 \sin^2\phi} \right) \right) \right) \tag{2.57}$$

Where CR is the ratio of the rod length and the crank radius, L_s is the stroke length, and ε the geometric compression ratio.

The dynamic cylinder volume V as a function of crank angle ϕ is obtained by multiplication with bore area as shown in (2.58). Differentiating V and multiplying with in-cylinder pressure gives the piston work.

$$V(\phi) = L_p(\phi) \cdot A_b = L_p(\phi) \cdot \frac{\pi}{4} D_b^2 \tag{2.58}$$

2.8 Heat Loss to Cylinder Walls

During combustion inside the cylinder a substantial part of the produced heat will be lost to the surrounding walls through convection. For the estimation of the amount of heat lost it is necessary to know the heat transfer coefficient α, the difference between the gas temperature T and the wall temperatures $T_{wall,i}$, and the total wall areas $A_{wall,i}$. Then the heat loss can be calculated according to (2.59) [Stapersma, 2010d].

$$\dot{Q}_{loss} = \sum_{i=1}^{3} \left\{ \alpha_{g \to w,i} \left(T - T_{wall,i} \right) A_{wall,i} \right\} \tag{2.59}$$

With $i = 1, 2, 3$ for respectively the cylinder walls, piston crown and the cylinder cover.

The wall temperatures are difficult to measure and therefore some assumptions have to be made. These temperatures are mean values, since the actual temperature profile along the walls will vary. The wall areas can easily be calculated from the stroke length and bore diameter as shown in (2.60) and (2.61).

$$A_{wall,1} = \pi D_b L_s \tag{2.60}$$

$$A_{wall,2} = A_{wall,3} = \frac{\pi}{4} D_b^2 \tag{2.61}$$

Estimation of heat transfer coefficients is a difficult task, and different semi-empirical formulas exist for this. In this thesis the Woschni formula will be used as shown in (2.62) [Stapersma, 2010d].

$$\alpha = 130 \cdot \frac{1}{D_b^{0.214}} \cdot \frac{p^{0.786}}{T^{0.525}} \cdot \left(C_3 \cdot c_m + C_4 \frac{p - p_0}{p_1} \cdot \frac{V_s}{V_1} \cdot T_1 \right)^{0.786} \tag{2.62}$$

Where p_0 is the cylinder pressure with no fuel injected, i.e. the engine is driven by an electric motor. The mean piston speed c_m and the stroke volume V_s is given in (2.63) and (2.64), respectively.

$$c_m = 2L_s n \tag{2.63}$$

$$V_s = \frac{\pi}{4} D_b^2 L_s \tag{2.64}$$

The constants C_3 and C_4 are related to the effect of swirl velocity w_t and the shape of the combustion chamber. For this thesis only the compression and expansion phase of the working stroke will be investigated, and since the diesel engine test bed has direct injection C_3 and C_4 are estimated as advised by Woschni [Stapersma, 2010b] and shown in (2.65) and (2.66).

$$C_3 = 2.28 + 0.308 \cdot \frac{w_t}{c_m} \tag{2.65}$$

$$C_4 = 0.00324 \left[\frac{\mathrm{m}}{\mathrm{s} \cdot \mathrm{K}} \right] \tag{2.66}$$

It is impossible to measure the swirl, but the ratio of swirl to mean piston speed was set to 10.

2.9 Engine Performance

To be able to say something about the performance of the engine it is necessary to look at mean cycle quantities rather than instantaneous values. The energy flow values of interest are the heat loss, heat input or indicated heat (heat from a T-s diagram), combustion heat flow (ROHR) and the indicated work (work from

a p-V diagram). The mean values can be calculated according to equations (2.67) - (2.70) [Ding, 2011].

$$\bar{\dot{Q}}_{loss} = \int_{IC}^{EO} \dot{Q}_{loss} \cdot \mathrm{d}t \cdot \frac{n}{k} \tag{2.67}$$

$$\bar{\dot{Q}}_{input} = \int_{IC}^{EO} \dot{Q}_{input} \cdot \mathrm{d}t \cdot \frac{n}{k} \tag{2.68}$$

$$\bar{\dot{Q}}_{comb} = \int_{IC}^{EO} \dot{Q}_{comb} \cdot \mathrm{d}t \cdot \frac{n}{k} \tag{2.69}$$

$$\bar{\dot{W}}_{indicated} = \int_{IC}^{EO} p \cdot \frac{\mathrm{d}V}{\mathrm{d}t} \cdot \mathrm{d}t \cdot \frac{n}{k} \tag{2.70}$$

Where n is the engine speed in [rev/s] and k is 2 for four-stroke engines and 1 for two stroke engines. The total engine efficiency is the ratio of useful work that the engine produces and the energy of the fuel. This efficiency can be broken down into partial efficiencies as shown in (2.71) [Stapersma, 2010a].

$$\eta_e = \eta_m \cdot \eta_{comb} \cdot \eta_{loss} \cdot \eta_{td} \tag{2.71}$$

Where η_m is the mechanical efficiency, η_{comb} the combustion efficiency, η_{loss} the heat loss efficiency and η_{td} the thermodynamical efficiency. These are the ratios presented in equations (2.72) - (2.75).

$$\eta_m = \frac{\dot{W}_e}{\dot{W}_i} \tag{2.72}$$

$$\eta_{td} = \frac{\dot{W}_i}{\dot{Q}_i} = \frac{\dot{W}_i}{\dot{Q}_{comb} - \dot{Q}_{loss}} \tag{2.73}$$

$$\eta_{loss} = \frac{\dot{Q}_i}{\dot{Q}_{comb}} = \frac{\dot{Q}_{comb} - \dot{Q}_{loss}}{\dot{Q}_{comb}} \tag{2.74}$$

$$\eta_{comb} = \frac{\dot{Q}_{comb}}{\dot{Q}_f} \tag{2.75}$$

Chapter 3

Test Set-Up And Models

3.1 Simulation Models

The models presented in this section are based on Stapersma [2010b],Stapersma [2010c] and Ding [2011]. A reaction rate signal is together with a constant engine speed the input to an in-cylinder process model. This model will calculate the in-cylinder temperature. The temperature can then be fed back into the model so that the pressure can be calculated from the gas law.

The overall in-cylinder process model is shown in Figure 3.1. The green input data block is where all the needed input data are set by the user. This will include engine speed, engine dimensions, initial conditions, fuel specifications, valve timing and Vibe parameters for the construction of reaction rate. The input parameters are distributed to where they are needed anywhere in the model. When the engine speed is integrated in time and converted the result is the crank angle which is the input to the cylinder volume function that calculates the in-cylinder volume. This volume is then differentiated and multiplied with pressure to give piston work. The in-cylinder volume is then the input to the gas law block which calculates the pressure.

The reaction rate is the input to the block "Mass and Air Fraction" which calculates the in-cylinder mass used in the gas law, and the in-cylinder air fraction. The air fraction is used for calculation of the thermodynamic properties in "Thermodynamic Properties" block. This block calculates the gas constant, heat of combustion, specific energy of fuel and the specific heat capacity at constant volume.

The heat loss to the walls is calculated in the "Heat Loss" block where the Woschni formula is used for the heat transfer coefficient estimation. Then all the terms needed in (2.1) are available and is arranged as shown in the figure to obtain the temperature which is fed back into the model. The integration block for the calculation of the temperature is given the start value T_1 which was set in the input block.

When the in-cylinder process model had an appropriate functionality, it was reversed to be able to calculate reaction rate based on a measured pressure. This model is shown in Figure 3.2. The lookup table contains the measured pressure points for every 0.5° crank angle. This means that the crank angle calculated from integration of the engine speed is input to the lookup table which will interpolate to give out the pressure in-between the measured points. Accordingly in the heat loss calculation block a lookup table is used for the measured pressure without fuel injection. The output from the heat release model is the reaction rate. When the reaction rate is integrated it gives the reaction co-ordinate. The RCO can be used to fit a Vibe function and thereby give the parameters needed to construct a new reaction rate signal that is smooth.

For running the models in the Simulink program some guidance is necessary. Simulation of pressure based on Vibe functions can be done in a file called "MODEL.slx". Vibe parameters and other specifications must be set in the input block.

If the wish is to have a measured pressure as the input and calculate whatever

desired parameter, the pressure and it corresponding crank angle must be loaded into the workspace in MATLAB before the simulation can start. Also a measured pressure without fuel injection is needed. These three measured values must be stored in the workspace in matrix form as respectively p, CA and $p0$. Then the file "ROHRMODEL.slx" can be run after setting the desired input parameters. The green input block must be double-clicked to open. The details for this can be found in Appendix D. Scopes from the model library in Simulink can be connected to whatever signal line and the signal progression can be viewed. The step-size is important, as it should not be too high or too low. With the maximum step size set to 0.00001, decent results are obtained.

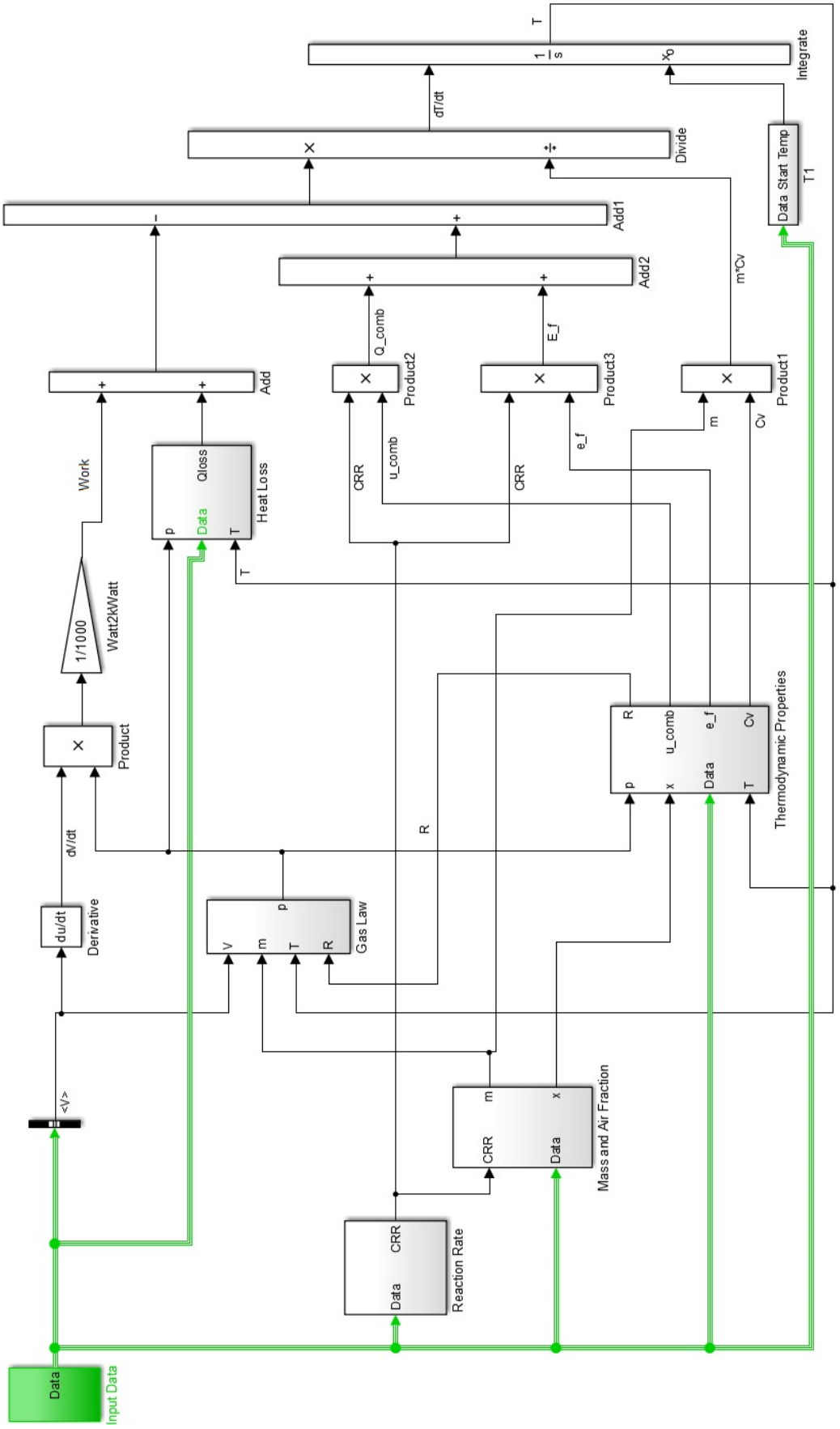

FIGURE 3.1: Overall in-cylinder process simulation model

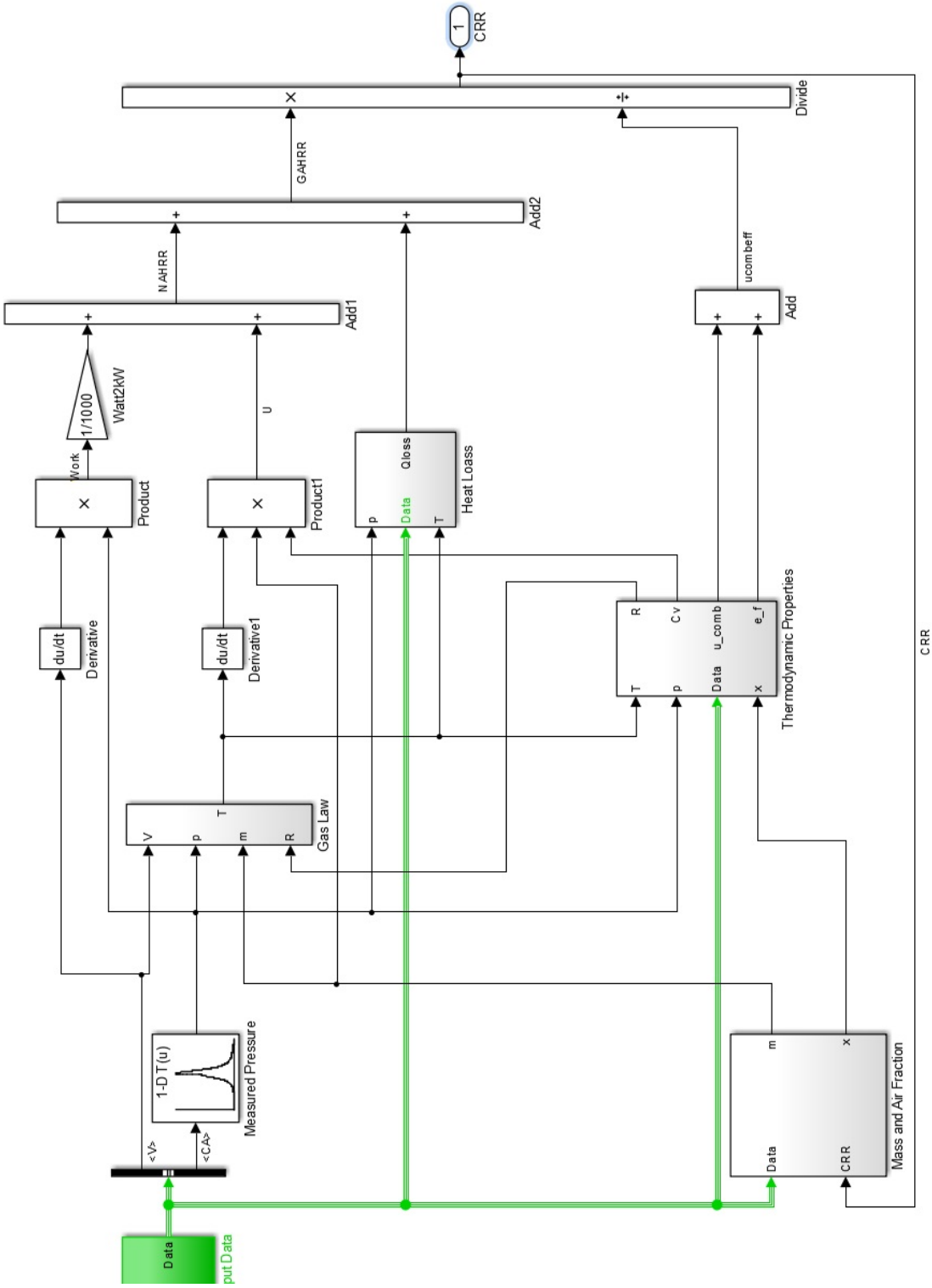

FIGURE 3.2: Overall heat release calculation model

3.2 Initial Conditions and Constant Parameters

The input parameters used in this thesis are based on an engine available in the Marine Machinery Laboratory at the Department of Marine Technology at Tyholt in Trondheim. This is a Ricardo Hydra test engine donated by Statoil. Engine specifications are presented in Table 3.1, while important assumed conditions are given in tables 3.2 and 3.3. Necessary information about the fuel type used for the testing can be seen in Table 3.4.

TABLE 3.1: Hydra test engine specifications

Parameter	Symbol		
Bore Diameter	D_b	78.35	[mm]
Stroke Length	L_s	88.90	[mm]
Connecting Rod Length	L_r	158	[mm]
Crank Throw Radius	R_c	44.45	[mm]
Crank/Rod Ratio	CR	0.2813	[-]
Compression Ratio	ε	19.5228[a]	[-]
Inlet Closes	IC	8	° ABDC
Exhaust Opens	EO	326	° ABDC
Maximum Power	P_{max}	8	[kW]
Maximum Speed	N_{max}	4500	[rpm]
Maximum Cylinder Pressure	p_{max}	120	[bar]
Fuel Injection	Common Rail,Piezoelectric		

[a]calculated value

TABLE 3.2: Initial conditions for Hydra test engine

Parameter		Unit
x_1	0.95[a]	[-]
p_1	1.0[b]	[bar]
T_1	347[b]	[K]
R_1	287	[J/kgK]

[a]assumed value
[b]rounded value

Since the test-bed at the time of testing did not have turbo-charging installed the trapped pressure is the atmospheric pressure which was set to 1 [bar] for simplicity. The trapped temperature was assumed to be the air temperature measured after

TABLE 3.3: Constant assumed values for Hydra test engine

Parameter		Unit
λ	2.0^a	[-]
T_{wall}	150^a	°C
T_{cover}	250^a	°C
T_{crown}	250^a	°C

[a]assumed value

TABLE 3.4: Properties of MGO[Halvorsen]

Property	MGO	
Density @ 15°C	830^a	[kg/m^3]
Sulfur	<5	[ppm]
x_C	0.8478	[-]
x_H	0.1495	[-]
x_O	0.0027	[-]

[a]Value assumed from properties of similar fuels

an air heater installed on the testing system which was 23.21 °C, plus an additional heat pickup in the inlet valve of 50 °C. V_1 is the cylinder volume at IC, calculated from the volume function explained in section 2.7. The trapped air fraction is set to 0.95, so that residual gases that were not scavenged are accounted for. The trapped mass m_1 can then be calculated according to the gas law as shown in (2.12).

3.3 Testing Procedure

For the Hydra test engine pressure measurements were taken for 8 working points. The working points are based on two defined ISO-standard load curves. One is representing a generator load that means keeping the engine speed constant while varying torque and the other represents a propeller load which means varying both engine speed and torque. For the propeller load curve the pressure is also measured at idle conditions. The tables 3.5 and 3.6 show the testing standards, with the calculated loads and engine speeds based on a rated speed of 1800 [rpm] and rated

torque of 28.8 [Nm]. Figure 3.3 illustrates the range over which the tests were done. The rated values are not the actual rated, but were set this way because there were problems with keeping the common rail pressure constant in addition to a leakage at the engine top. This was done because it was undesirable to exert the engine in this condition to heavy loads. Notice that the working points 11 and 21 are the same.

TABLE 3.5: Generator loading curve

Working Point	WP_{11}	WP_{12}	WP_{13}	WP_{14}	
ISO-standard speed	100	100	100	100	[%]
Speed for Hydra test	30	30	30	30	[rps]
ISO-standard torque	100	75	50	25	[%]
Torque for Hydra test	28.8	21.6	14.4	7.2	[Nm]

TABLE 3.6: Propeller loading curve

Working Point	WP_{21}	WP_{22}	WP_{23}	WP_{24}	WP_{25}	
ISO-standard speed	100	91	80	63	Idle	[%]
Speed for Hydra test	30	27.3	24	18.9	16	[rps]
ISO-standard torque	100	75	50	25	0	[%]
Torque for Hydra test	28.8	21.6	14.4	7.2	0	[Nm]

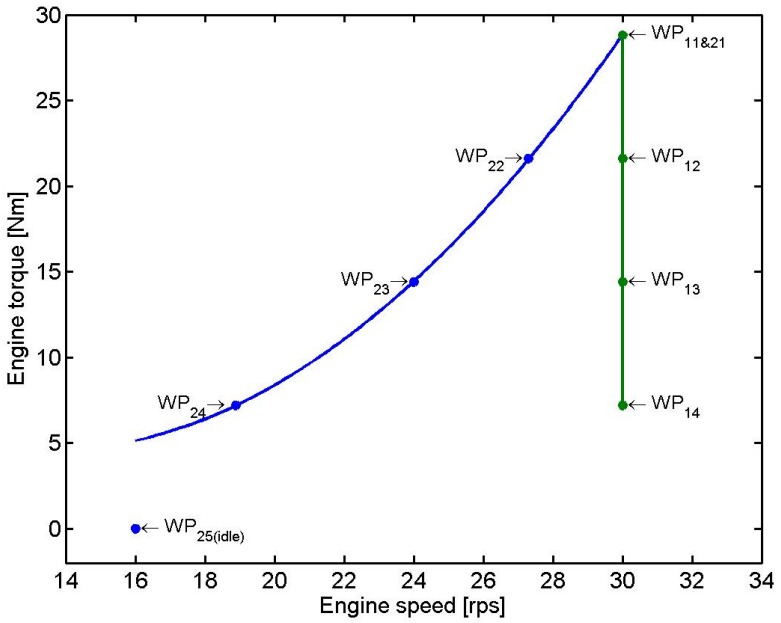

FIGURE 3.3: Generator and propeller load working points for Hydra test engine

Chapter 4

Results

4.1 Results From Raw Data

The equations used are valid from the inlet closes to the exhaust opens condition so the simulations that were carried out start and end at these crank angles.

4.1.1 Pressure Measurements

The pressure measurements were taken for 20 cycles and the averaged results for the generator load and propeller load are shown in Figure 4.1. This is the raw data and some fluctuations in the pressure trace are present. Since this shows the averaged measurements, and the step-size in the simulation environment can be set as short as desired the graphs show little fluctuations. It is clear that a higher load gives a higher pressure peak. The pressure was also measured when there was no fuel injected to the cylinder. These pressures increase with higher speeds.

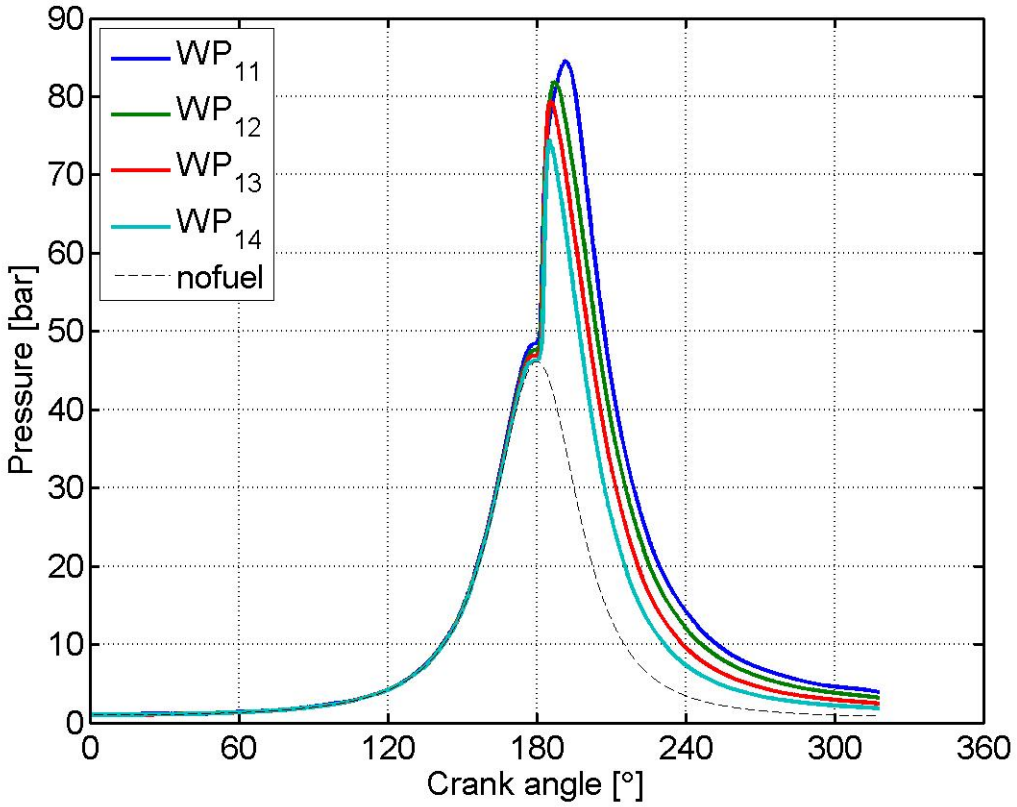

(a) Generator load

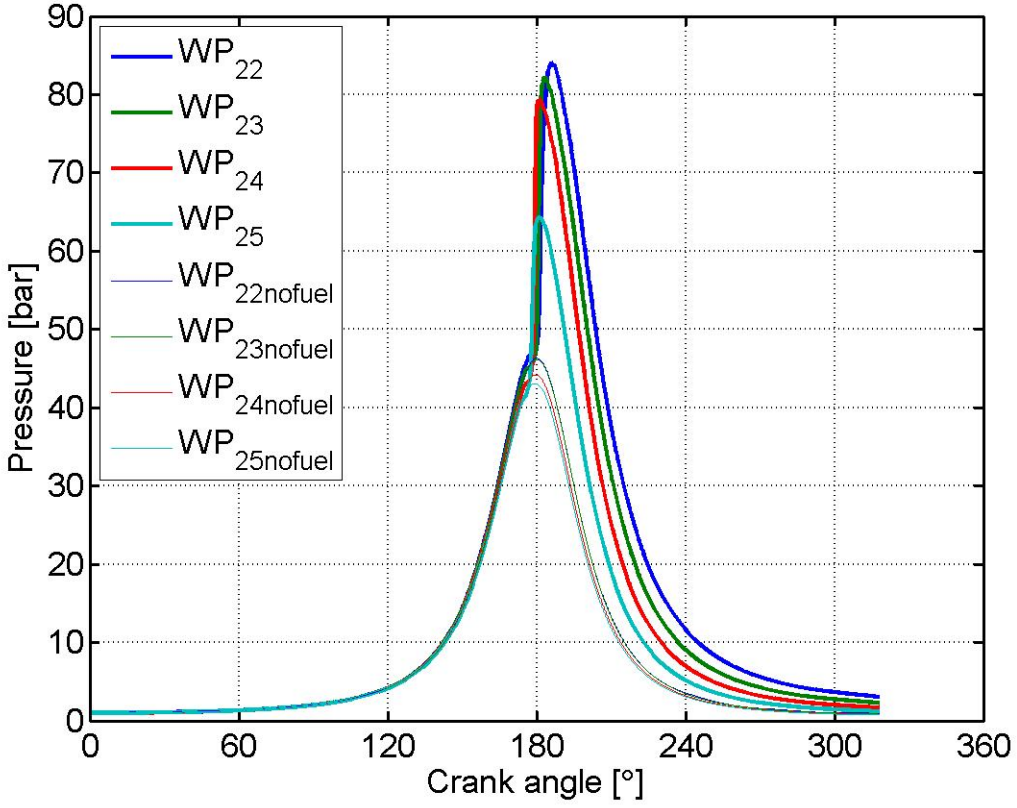

(b) Propeller load

FIGURE 4.1: Measured cylinder pressures for Hydra test engine

4.1.2 Combustion Reaction Rate

The reaction rates calculated by the heat release model are shown in Figure 4.2. The ordinate axis shows time instead of crank angle, with the purpose of better illustrating each working point. However, when the engine speed is kept constant the graphs lay somewhat on top of each other. Fluctuations can be seen due to the differentiations in the calculation procedure, which amplifies the small fluctuations in the pressure measurements. For WP_{11} the premixed combustion phase pressure peak is a little lower than for the other working points, but a peak in the diffusive combustion phase can be noticed. Higher loads seem to give higher peaks for the diffusive combustion phase. For idle conditions the reaction rate has a lower premixed combustion pressure peak and no diffusive combustion.

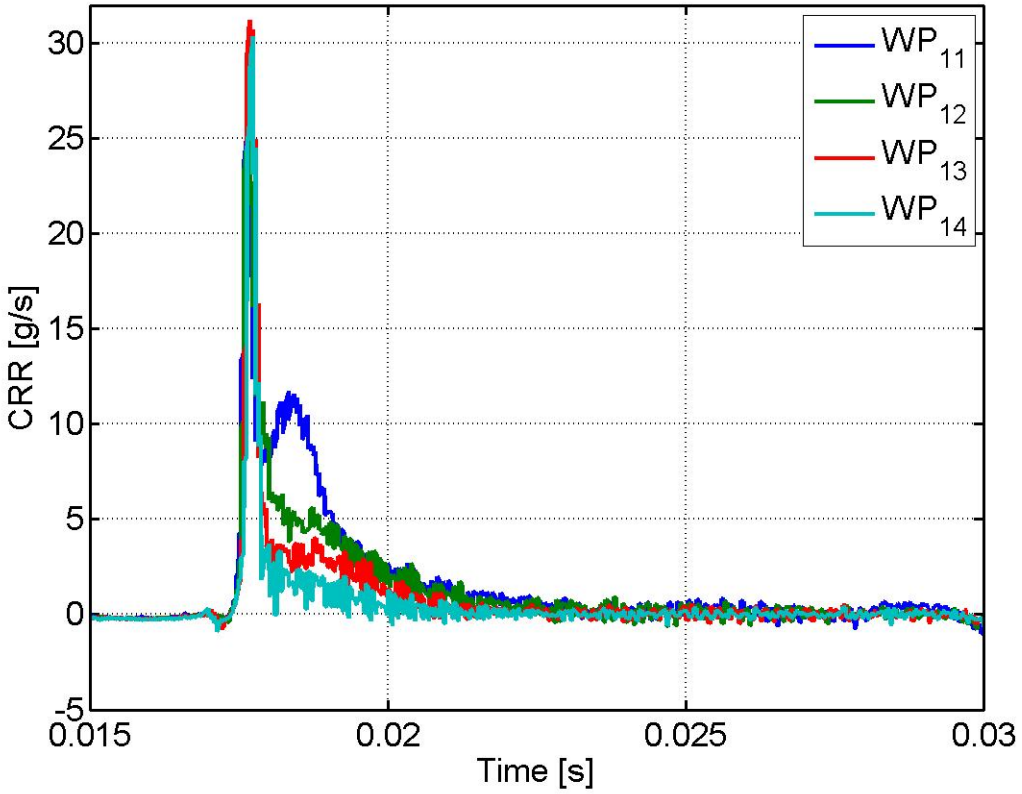

(a) Generator load

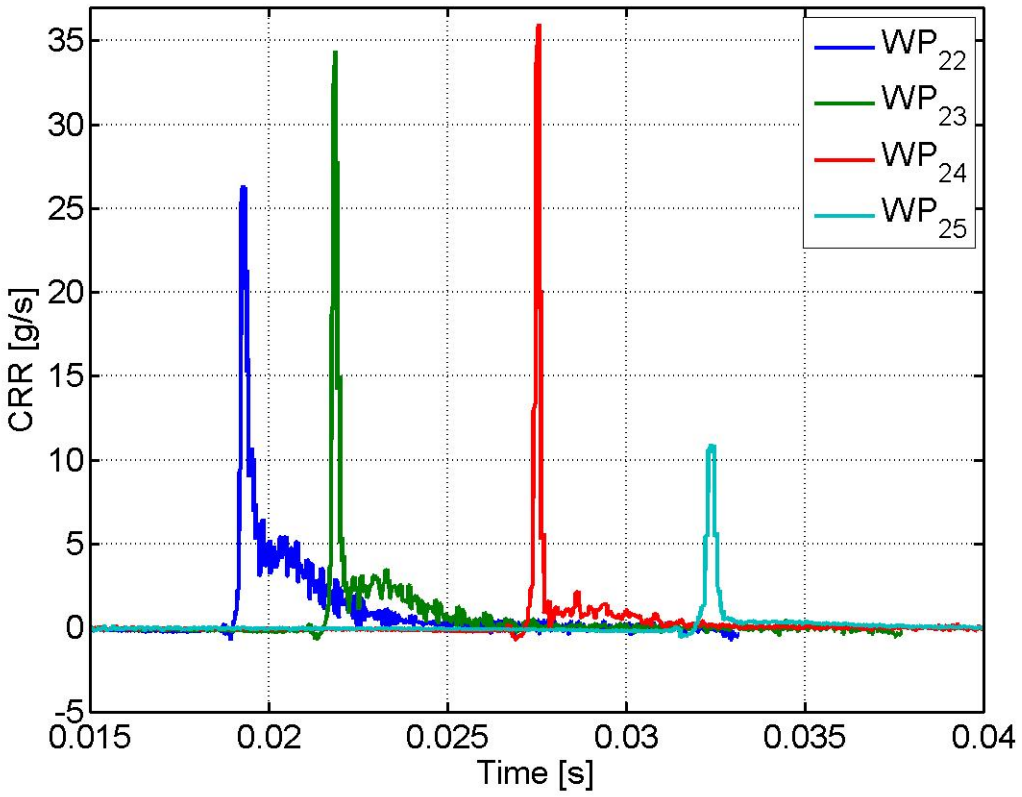

(b) Propeller load

FIGURE 4.2: Calculated reaction rates

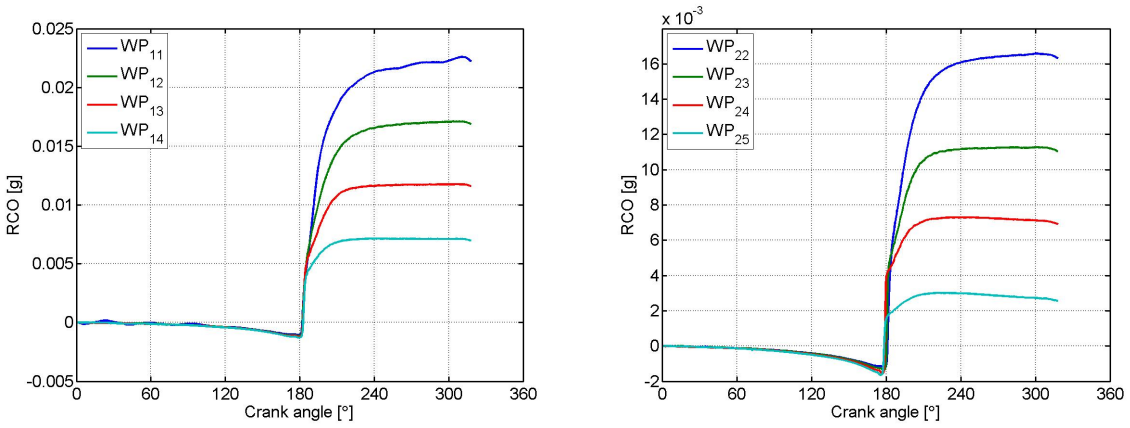

(a) Generator load

(b) Propeller load

FIGURE 4.3: Calculated reaction co-ordinates

In section 4.3 a method for smoothing the fluctuating nature of the reaction rate signal will be explained. The method involves curve fitting of the calculated RCO shown in Figure 4.3. For the RCO signals a dip before SOC can be seen and this is not physical. Since no fuel is present the RCO should be 0 until the start if injection. If the RCO is negative it means that fuel is being created, which is impossible.

4.1.3 Combustion Heat Flow (ROHR)

The instantaneous combustion heat flow or rate of heat release is shown in Figure 4.4. Also here a dip before SOC can be noticed, but this is because the fuel is evaporating and therefore consumes energy instead of releasing it. The instantaneous heat flow shows the same trend as the reaction rate. When the energy of the entering liquid fuel $\dot{E}$ is included the effective instantaneous heat flows become a little lower as shown by the continuous lines.

The mean combustion heat is shown in Figure 4.5. Also for the mean combustion heat the unphysical dip before SOC can be recognized. It seems that the difference between the effective combustion heat and the combustion heat before adding $\dot{E}$ is greater at higher loads, speeds and thus temperatures.

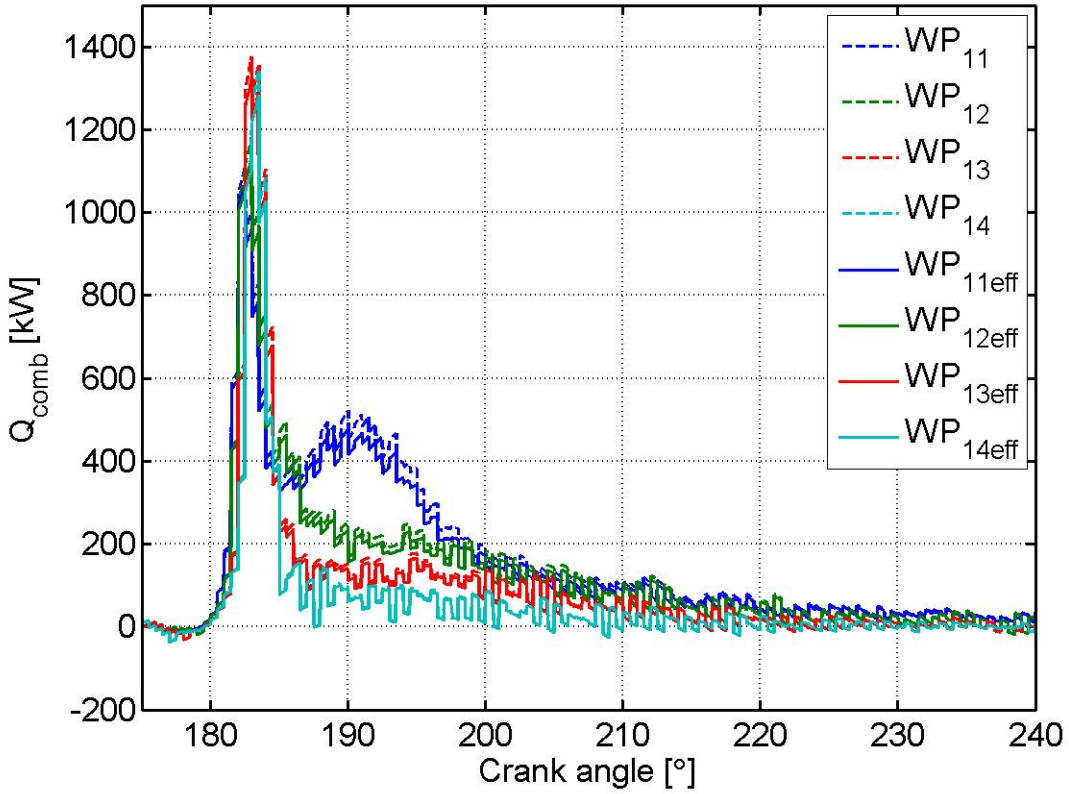

(a) Generator load

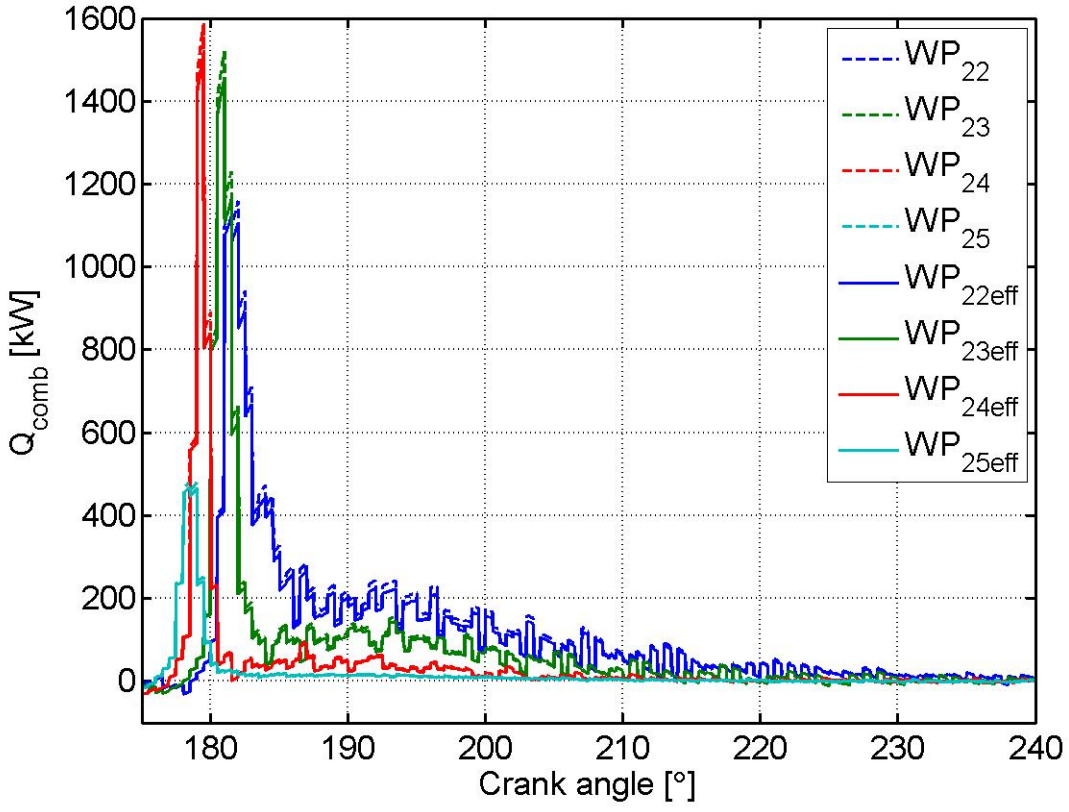

(b) Propeller load

FIGURE 4.4: Calculated instantaneous combustion heat flows

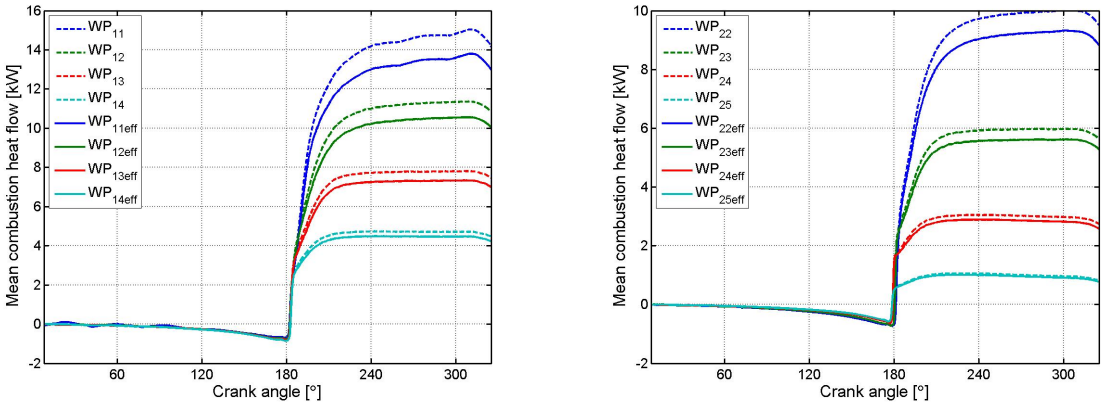

(a) Generator load (b) Propeller load

FIGURE 4.5: Calculated mean combustion heat flows

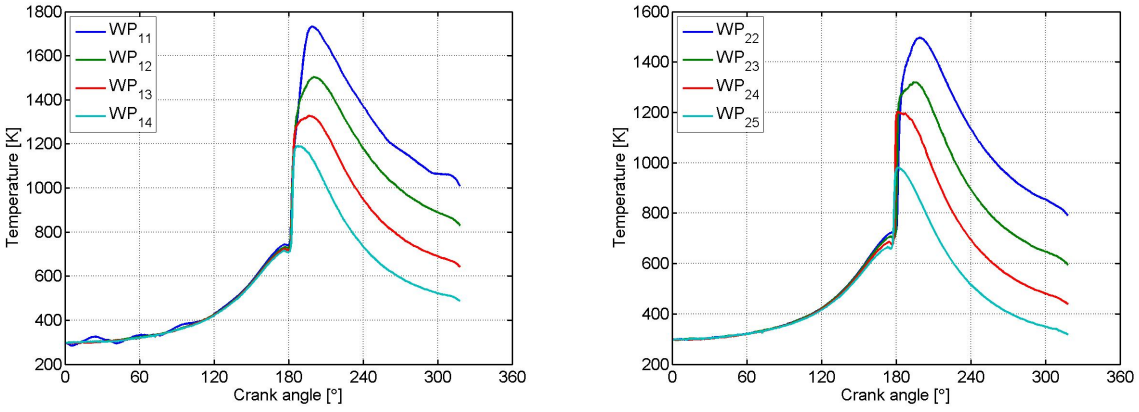

(a) Generator load (b) Propeller load

FIGURE 4.6: Calculated in-cylinder temperatures

4.1.4 In-Cylinder States

As shown in Figure 4.6 the temperatures increase with heavier loads and higher speeds. The cylinder volume calculated from (2.58) for the Hydra is shown in Figure 4.7. Calculated in-cylinder masses are shown in Figure 4.8. They start at m_1 and increases when fuel is injected. More fuel has to be injected with heavier loads and higher speeds. The same dip before SOC as for the RCO can be recognized for the in-cylinder mass. The in-cylinder air fraction gets an increase before the SOC because its calculation includes the RCO. It is clear from the graphs that more air is consumed with heavier loads and higher engine speeds.

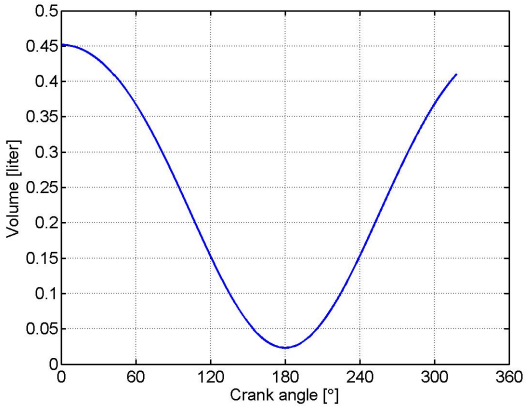

FIGURE 4.7: Calculated in-cylinder volume

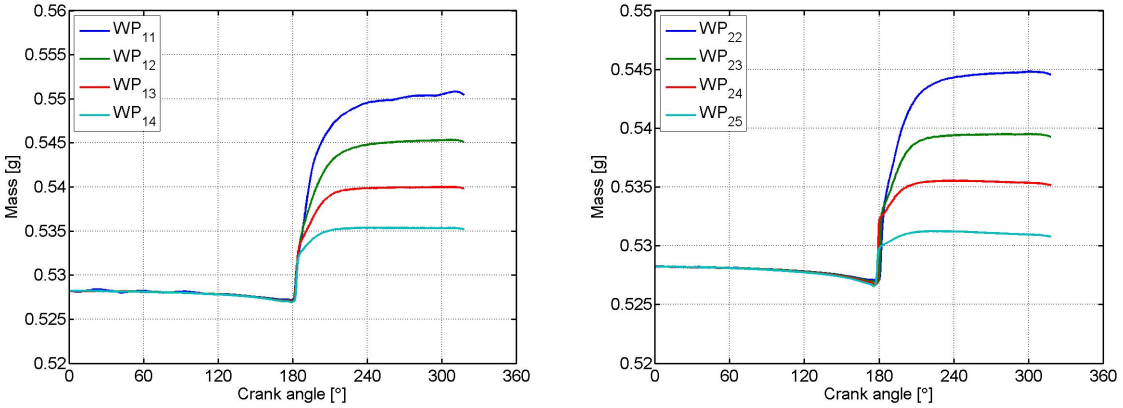

(a) Generator load (b) Propeller load

FIGURE 4.8: Calculated in-cylinder masses

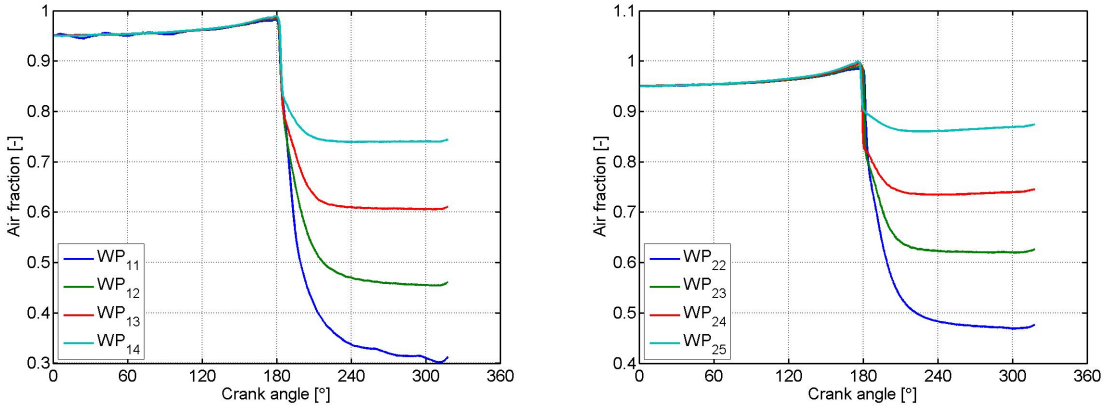

(a) Generator load (b) Propeller load

FIGURE 4.9: Calculated in-cylinder air fractions

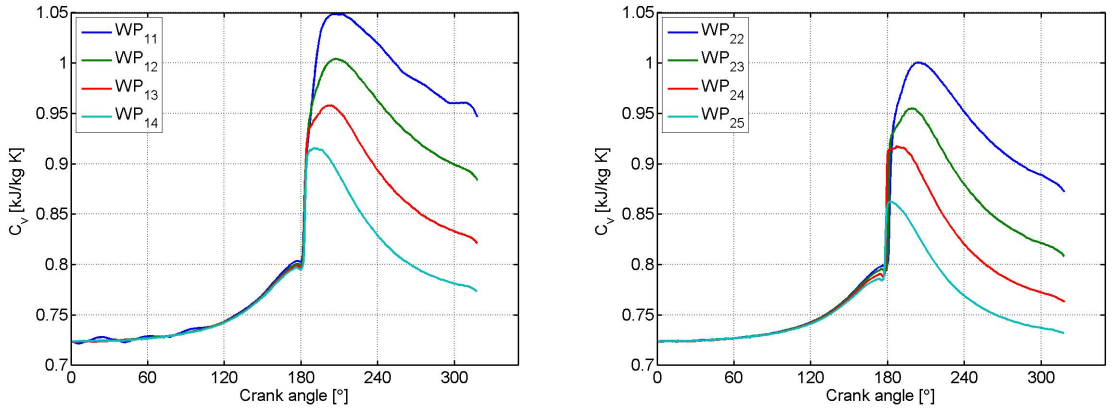

(a) Generator load (b) Propeller load

FIGURE 4.10: Specific heat capacities at constant volume

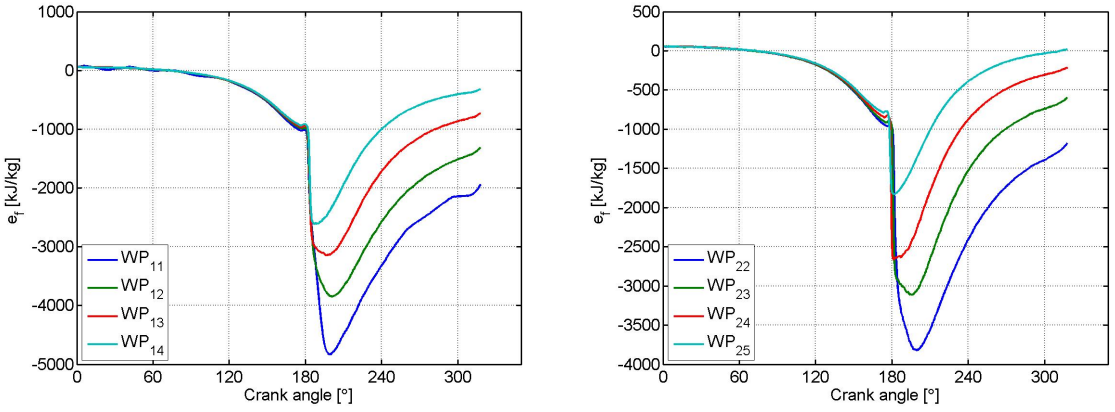

(a) Generator load (b) Propeller load

FIGURE 4.11: Specific energies of liquid fuel

4.1.5 Thermodynamic Properties

The thermodynamic properties for the cylinder gas is somewhere in between the properties of dry air and stoichiometric gas. From Figure 4.10 it is clear that the specific internal energies at constant volume are dominated by their temperature dependency. Figure 4.11 shows the specific energies of the entering liquid fuel. These energies decrease with temperature because energy is consumed in the evaporation process. When the specific heats of combustion u_{comb} of the gaseous fuel are added to these energies, the effective specific heats of combustion are decreased with increasing temperatures as shown by the continuous lines in Figure 4.12.

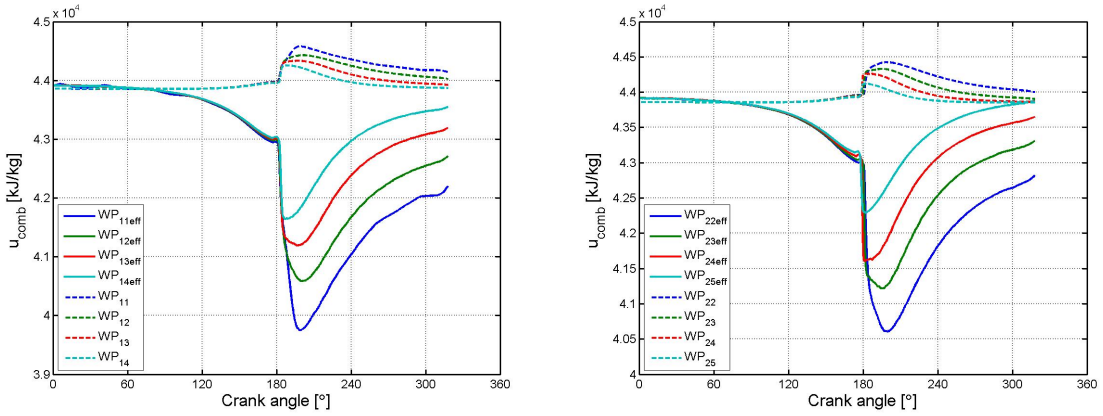

(a) Generator load (b) Propeller load

FIGURE 4.12: Specific heats of combustion

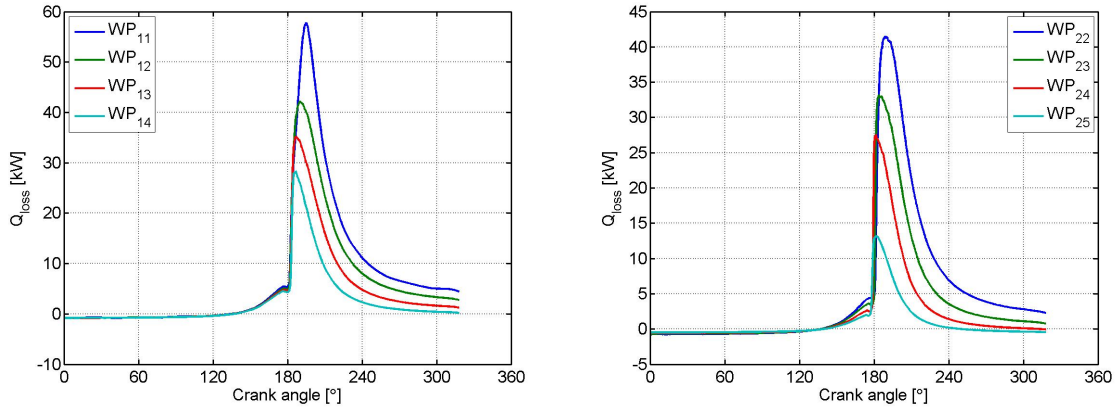

(a) Generator load (b) Propeller load

FIGURE 4.13: Calculated heat losses

4.1.6 Heat Loss

Increased engine speeds and loads give increased heat loss to the walls. Both the heat transfer coefficients and the heat loss flows follow the trend of the pressure. For the propeller load curve which changes speed it can be seen that the differences at SOC is bigger than for the generator load. The estimation of the heat transfer coefficient includes the mean piston speed, which again depends on the engine speed, so that might explain this. At the start of compression (IC) the heat loss is negative, which means that the gas is picking up heat from the then hotter cylinder walls. The mean heat losses are shown in Figure 4.15.

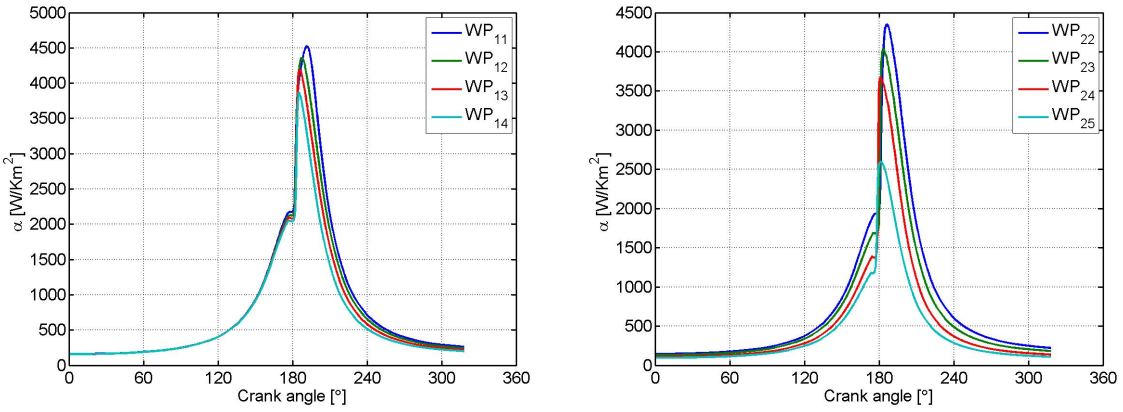

(a) Generator load (b) Propeller load

FIGURE 4.14: Calculated heat transfer coefficients

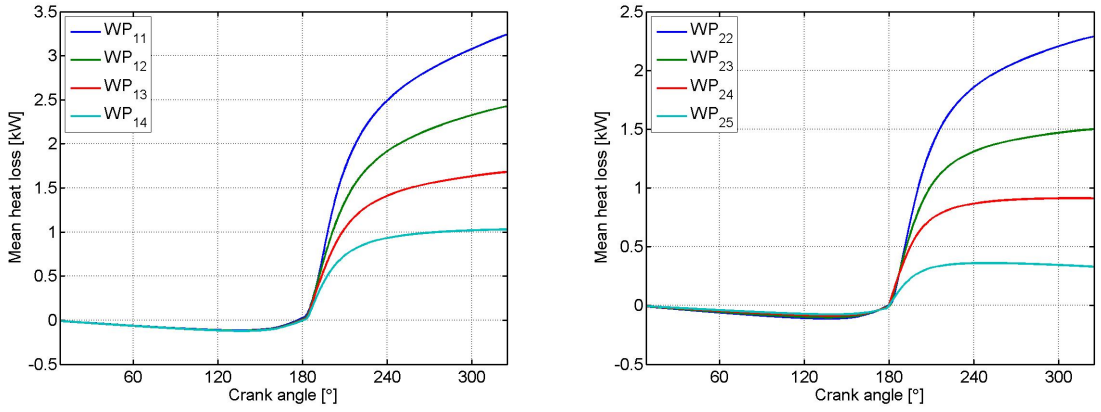

(a) Generator load (b) Propeller load

FIGURE 4.15: Calculated mean heat losses

4.1.7 Indicated Work

The instantaneous indicated work for the 8 working points is shown in Figure 4.16, while the mean indicated power as calculated from (2.70) is shown in Figure 4.17. Since the compression requires energy, the work is negative until the top dead center (TDC). With increasing speed the required work is greater because the compression must happen faster. When the loads increase more work is done in the expansion phase. The mean indicated power of the engine is shown in Figure 4.17. When mechanical losses are accounted for through the mechanical efficiency, this will give the actual output power on the engine shaft.

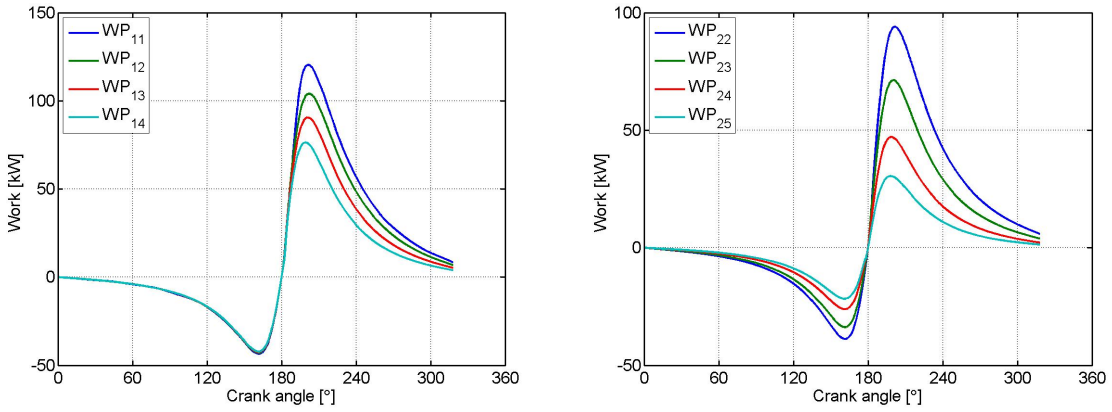

(a) Generator load (b) Propeller load

FIGURE 4.16: Calculated instantaneous indicated work

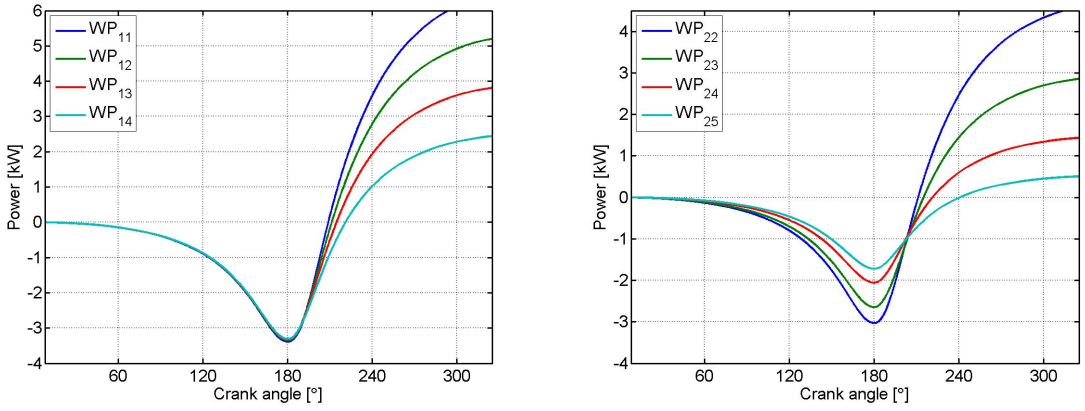

(a) Generator load (b) Propeller load

FIGURE 4.17: Calculated mean indicated power

4.1.8 Engine Performance

With the measured shaft power on the Hydra known, it was possible to calculate the engine performance. Table 4.1 shows the measured shaft power and the calculated mean energy flows. The calculated efficiencies of the engine are shown in Table 4.2.

The mechanical efficiencies decrease with decreasing loads and speeds. This means that more energy is lost to driving the oil pump, camshaft, valves and friction etc. with lower loads and speeds. For the thermodynamical efficiency the tendency is that it gets higher with decreasing load and speed.

TABLE 4.1: Caclulated energy flows for the Hydra test engine

(a) Generator load

(b) Propeller load

	WP_{11}	WP_{12}	WP_{13}	WP_{14}	WP_{22}	WP_{23}	WP_{24}	WP_{25}	
P_{shaft}	5.42	4.14	2.75	1.31	3.70	2.13	0.89	0.08	[kW]
$P_{indicated}$	6.48	5.21	3.82	2.45	4.58	2.86	1.44	0.51	[kW]
Q_{loss}	13.80	10.56	7.34	4.49	2.29	1.50	0.91	0.36	[kW]
Q_{comb}	13.97	10.59	7.36	4.25	9.33	5.62	2.89	1.01	[kW]

TABLE 4.2: Caclulated efficiencies for the Hydra test engine

(a) Generator load

(b) Propeller load

	WP_{11}	WP_{12}	WP_{13}	WP_{14}	WP_{22}	WP_{23}	WP_{24}	WP_{25}
η_m	0.836	0.794	0.721	0.536	0.807	0.743	0.618	0.155
η_{td}	0.614	0.641	0.675	0.707	0.651	0.694	0.727	0.778
η_{loss}	0.765	0.770	0.771	0.771	0.754	0.733	0.684	0.643
η_e	0.393	0.392	0.375	0.292	0.396	0.378	0.307	0.078

The heat loss efficiency seems to be affected mostly by engine speed, since it decreases with lower speed. The overall efficiency is best at WP_{13}. Since the working points are based on a speed which is not the actual rated speed, these efficiencies unfortunately do not give a broad picture of the engine performance. At idle conditions some load is measured because it was not possible to disconnect the generator from the engine shaft.

4.2 Causes Of Impossible Results

The calculated RCOs show results that are not physically possible. First of all the RCO should be constant and equal to 0 until the SOC. As can be seen in the figures this is not the case. This will influence all values that are calculated based on the RCO. This could be caused by the uncertainty in the calculation of the heat transfer coefficient calculated by the semi-empirical Woschni equation.

Other reasons can be errors in the measurement of the crank angle and the pressure. Especially in the pressure measurement there could be errors because the pressure sensor only measures a pressure difference, and has to be shifted to a certain absolute pressure. A third influencing factor could be that the compression ratio is different from the presented value. The seals in the cylinder can be compressed so that the cylinder volume increases. There is also the possibility that a layer of matter forms at some of the walls also changing the cylinder volume. Changes in the cylinder volume at such small engines could possibly have an influence.

To see the influence of these four factors some shifting was done. First the influence of changing the heat transfer coefficient α was carried out by running through the program and multiply α with a factor A ranging from 0.5 to 1.5. Then the measured crank angle and measured pressure were given shift ranging from -0.5 [°] to +0.5 [°] and -0.5 [bar] to +0.5 [bar], respectively. Lastly the effect of shifting the compression ratio with a range of -1 to +1 was investigated. The effects on the RCOs are shown in the figures 4.18 - 4.21.

Changing the heat transfer coefficient does not seem to affect the dip before SOC to a great extent. Figure 4.18 shows that more fuel is burned if the heat loss coefficient is increased. This is reasonable because if more heat energy is lost, more fuel must be combusted to maintain the same power output.

Shifting the measured crank angle seems to have a minor effect on the RCO, but some differences are noticed. Figure 4.19 shows that more fuel is used when the crank angle is shifted in the positive direction.

It seems that shifting the measured pressure has the biggest influence. Figure 4.20 shows that with a shift of -0.25 [bar] the RCO seems more physically correct as it has moved the SOC closer to zero. This could be due to a pressure drop from where the pressure is measured, to where compression starts.

Changing the compression ratio also have the influence of moving the dip upwards with smaller ε. The shifts used here are large, and meant for indicating tendencies. Considering that the compression volume is known for the Hydra with an accuracy of 0.1 [cm^3], the impact does not seem to be very big.

The effects of shifting these values on several other outputs are shown in Appendix C.

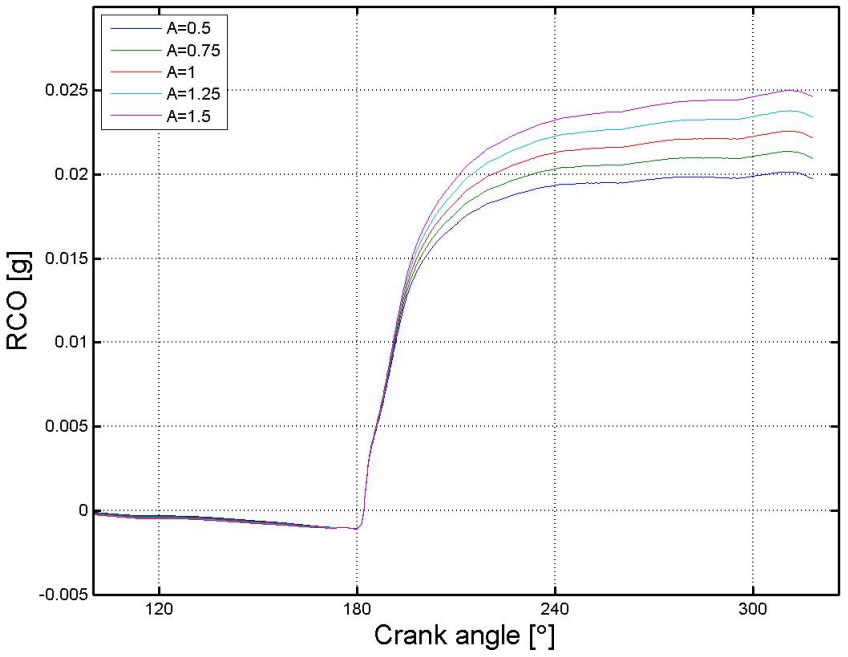

FIGURE 4.18: Effect of changing the heat transfer coefficient on the reaction co-ordinate at WP_{11}

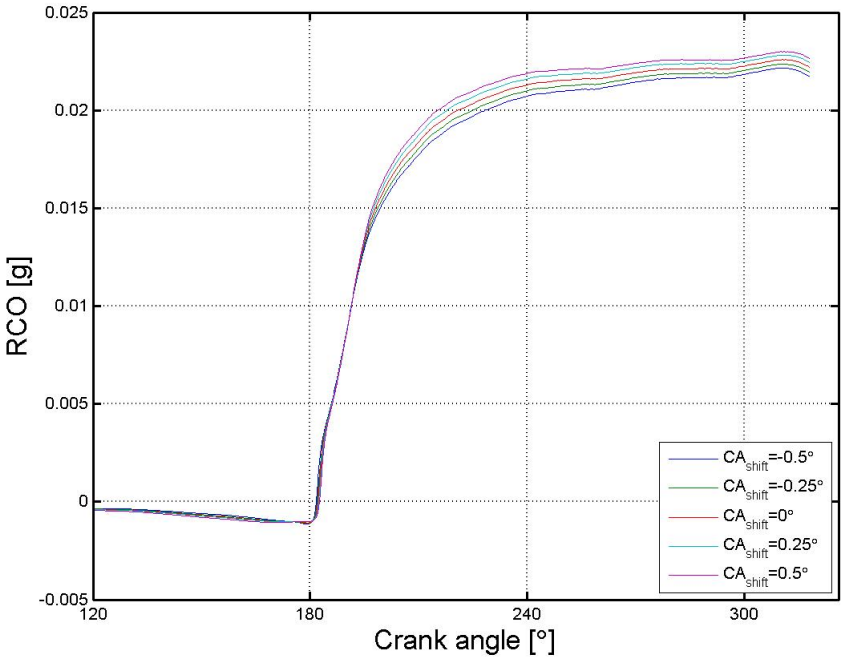

FIGURE 4.19: Effect of shifting the measured crank angle on the reaction co-ordinate at WP_{11}

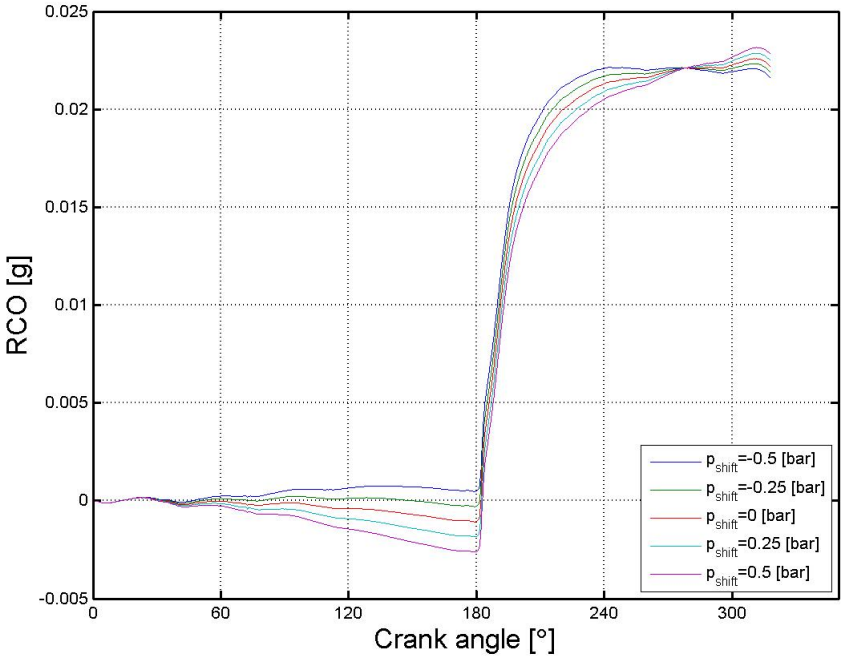

FIGURE 4.20: Effect of shfiting the measured pressure on the reaction co-ordinate at WP_{11}

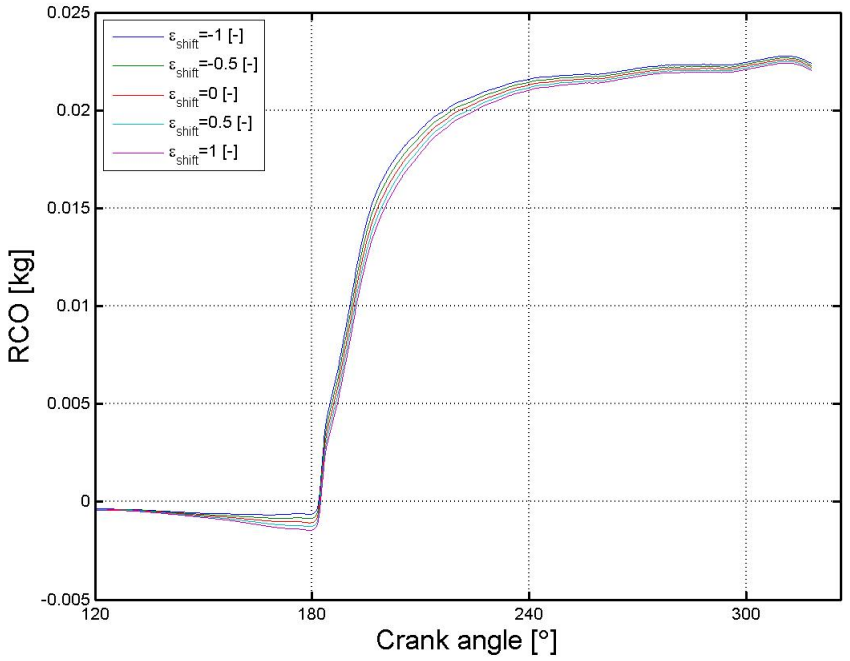

FIGURE 4.21: Effect of shfiting the compression ratio on the reaction co-ordinate at WP_{11}

4.3 Smoothing

Usually pressure measurements will have fluctuations that will be greatly amplified in the calculation of the combustion reaction rate. However, through the use of a smoothing technique involving curve fitting it is possible to find the appropriate Vibe parameters and construct a new reaction rate signal that is smoother.

4.3.1 Smoothing Attempt

The smoothing attempt started with shifting the pressure until the RCO seemed more physically logical. Then the SOC and EOC were estimated by reading the RCO signal calculated from the raw data. The SOC was assumed to be at the point where the rapid increase in the RCO signal was noticed and crossed zero. Estimating the EOC is difficult, but it was assumed to be when the RCO reaches its maximum. However, with values for SOC and EOC the non-dimensional time

TABLE 4.3: Vibe parameter values calculated by curve fitting toolbox

Coefficient	WP_{11}	WP_{14}	WP_{24}	
SOC	181	181	177.5	°
EOC	309.5	220.5	216	°
m_1	1.819	0.0001163	1.665	[-]
m_2	0.1439	2.172	0.2226	[-]
b_1	0.06196	0.7924	0.7493	[-]
b_2	0.9275	0.1961	0.2226	[-]
a	14.04	10.82	1592	[-]

can be calculated. The calculated RCO can be normalized and a curve fitting toolbox in MATLAB can be used to fit a Vibe function and thus the Vibe parameters can be used to construct a new and hopefully improved CRR signal.

It proved to be hard to get good fits, and this probably has to do with the selection of start values in the toolbox. It is necessary to have some experience with regard to this. However, the fits that were obtained for WP_{11}, WP_{14} and WP_{24} are shown in the figures 4.22 -4.27. The pressures for these working points were first shifted with respectively -0.3, -0.4 and -0.5 [bar]. The double Vibe parameters calculated for the fits are shown in Table 4.3 together with the respective SOC and EOC.

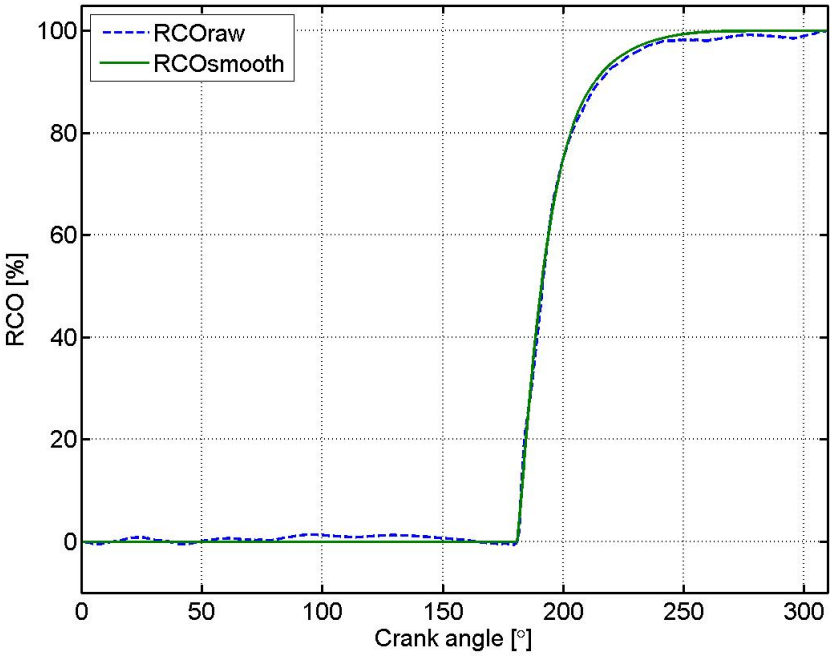

FIGURE 4.22: Vibe constructed RCO for WP_{11}

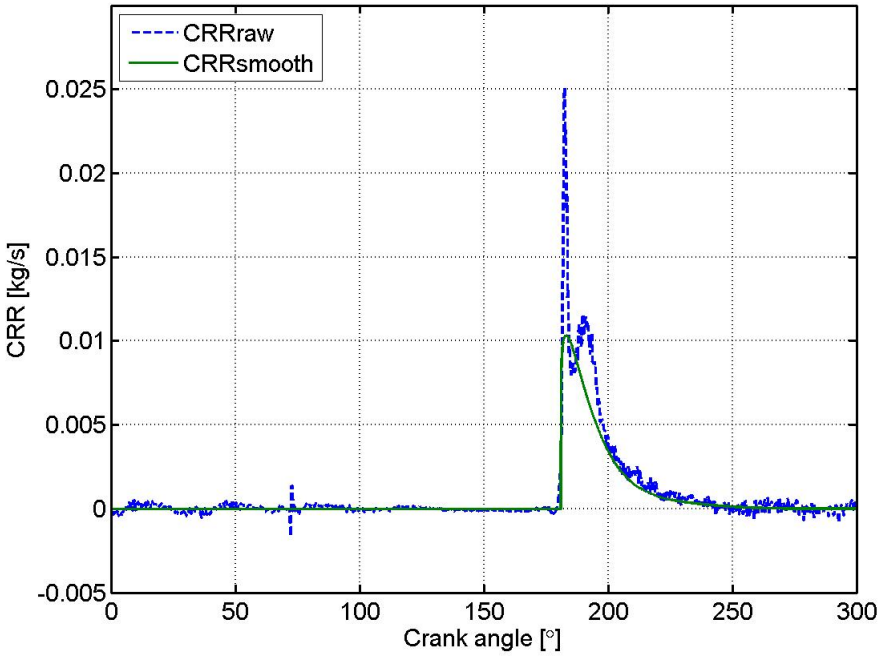

FIGURE 4.23: Vibe constructed CRR for WP_{11}

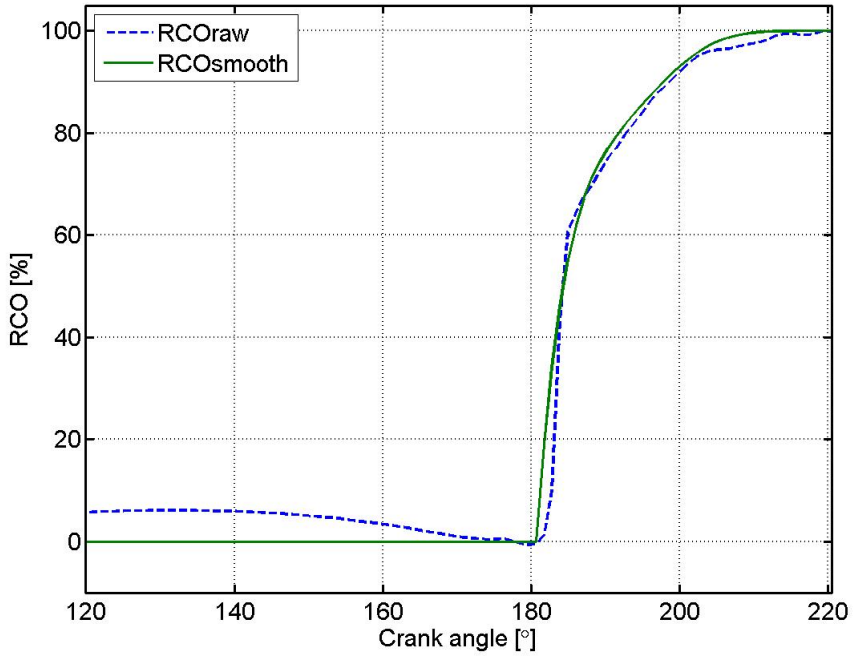

FIGURE 4.24: Vibe constructed RCO for WP_{14}

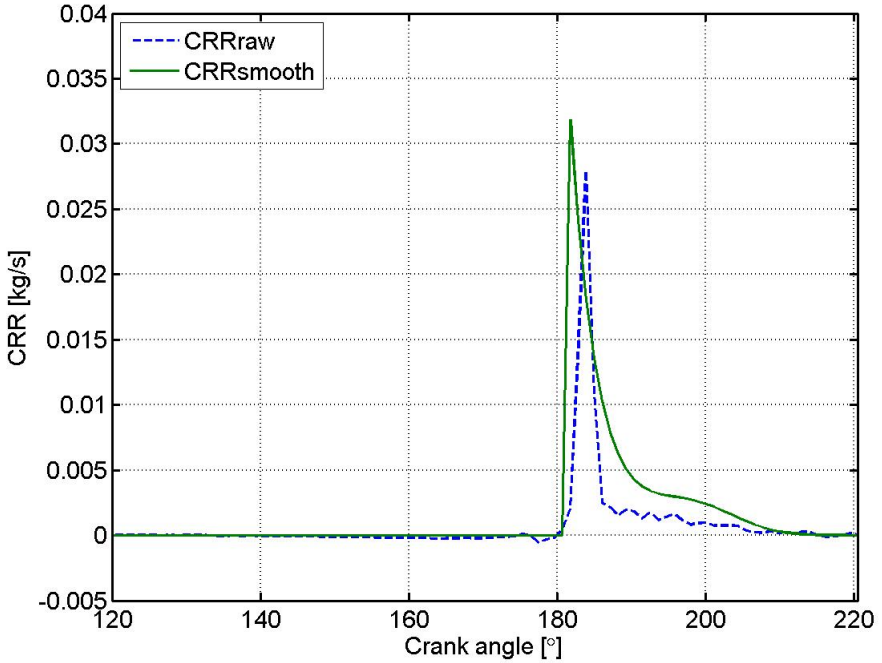

FIGURE 4.25: Vibe constructed CRR for WP_{14}

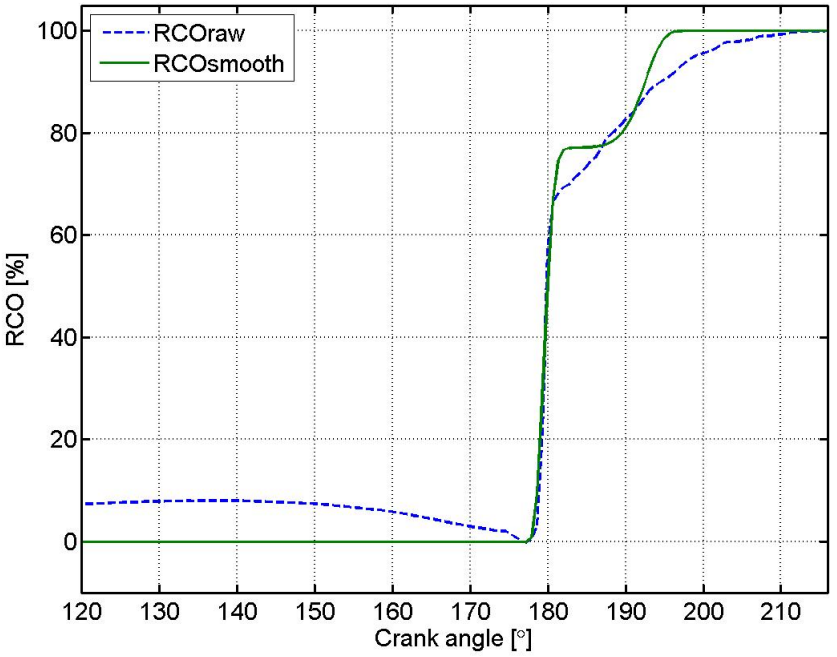

FIGURE 4.26: Vibe constructed RCO for WP_{24}

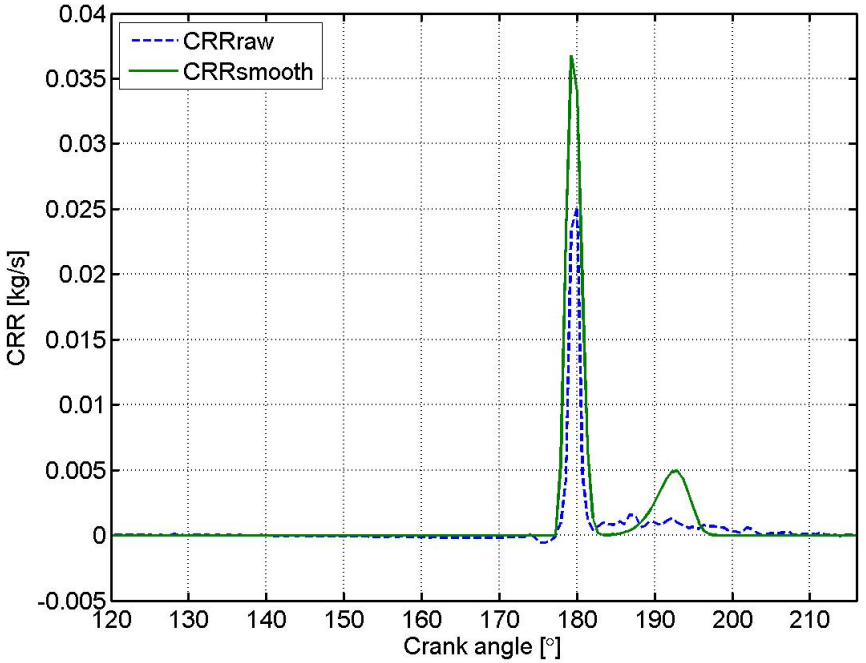

FIGURE 4.27: Vibe constructed CRR for WP_{24}

As shown in the figures the curve fits are poor. For WP_{11} the Vibe CRR ignores the spiky peak of the premixed combustion and the diffusive burning phase. For

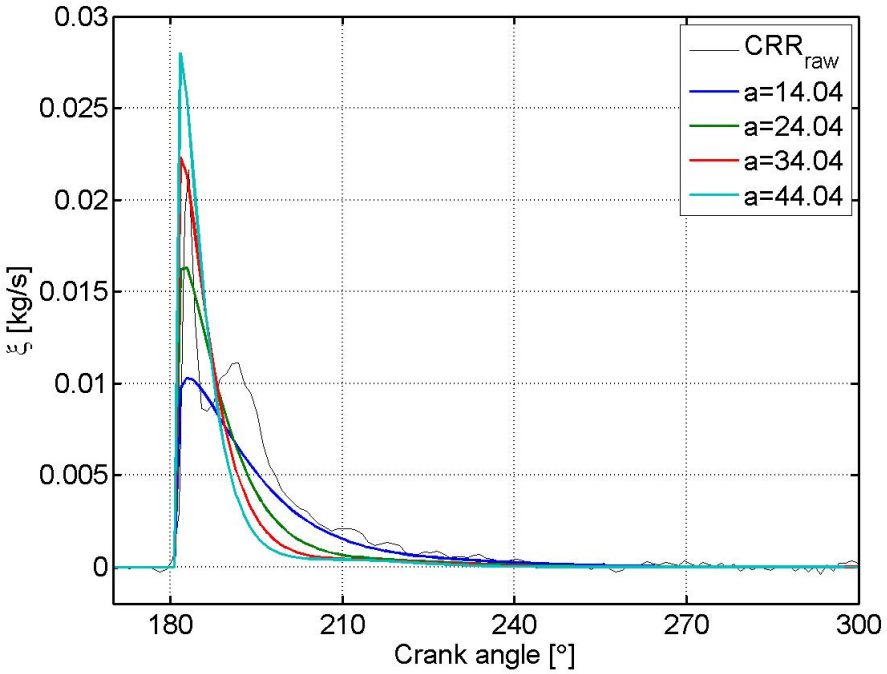

FIGURE 4.28: Changing paramter a for the Vibe function

WP_{24} the fit is getting some strange fluctuations between 70% and 100% burnt fuel, which of course makes the CRR fits bad. It was decided to leave the fits this way due to lack of time, but the influence of changing the different Vibe parameters with the values in Table 4.3 as a starting point will be presented in section 4.3.2.

4.3.2 Manually Changing Vibe Parameters

Changing the consecutive Vibe parameters one at a time while keeping the others constant will show how the parameters impact the reaction rate. The figures 4.28 - 4.32 show the results for WP_{11}. The CRR calculated from raw measurements for WP_{11} is also shown in the graphs for comparison.

First the parameter a was varied as shown in Figure 4.28. The peak of the reaction rate becomes higher when this parameter is increased.

Next b_1 was varied while the a was held constant and equal to 38.54, since the peak

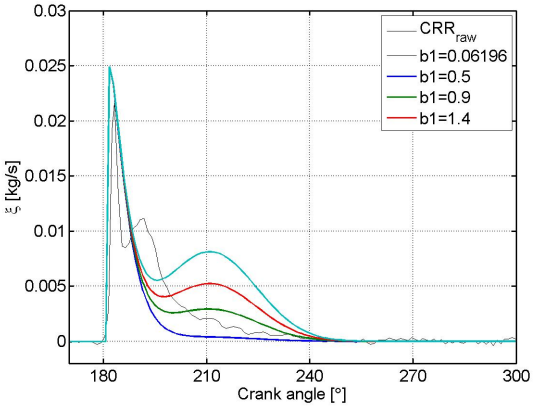

FIGURE 4.29: Changing paramter b_1 for the Vibe function

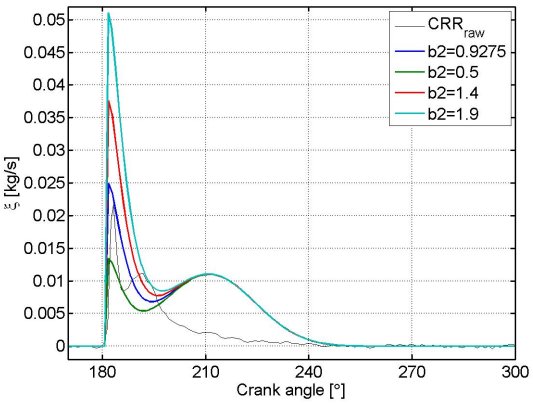

FIGURE 4.30: Changing paramter b_2 for the Vibe function

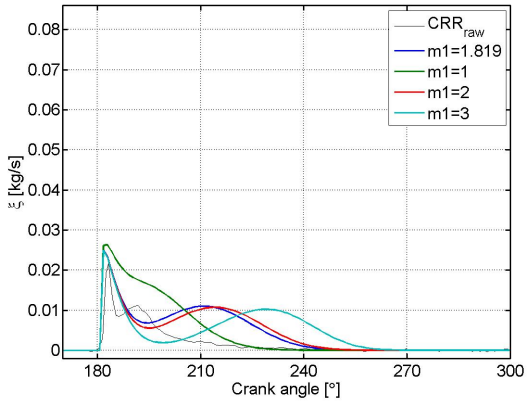

FIGURE 4.31: Changing paramter m_1 for the Vibe function

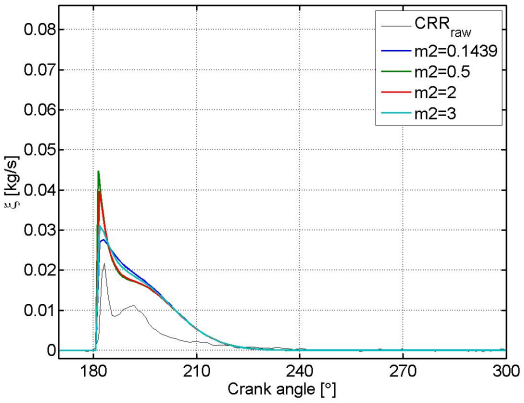

FIGURE 4.32: Changing paramter m_2 for the Vibe function

of the Vibe CRR were somewhat near the raw data CRR. The variation of b_1 is shown in Figure 4.29. It is clear that the peak of the diffusive phase of combustion goes up when b_1 is increased.

Setting b_1 to 1.9, a still 38.54 and changing b_2 gave the result as shown in Figure 4.30. The peak for the premixed combustion phase gets higher when b_2 is increased.

Changing m_1 moves the peak for the diffusive phase as shown in Figure 4.31.

Setting m_1 to 0.9 and changing m_2 gives the result as shown in Figure 4.32. This means that changing m_2 moves the peak of the premix phase. A smaller m_2 gives a more spiky premixed peak.

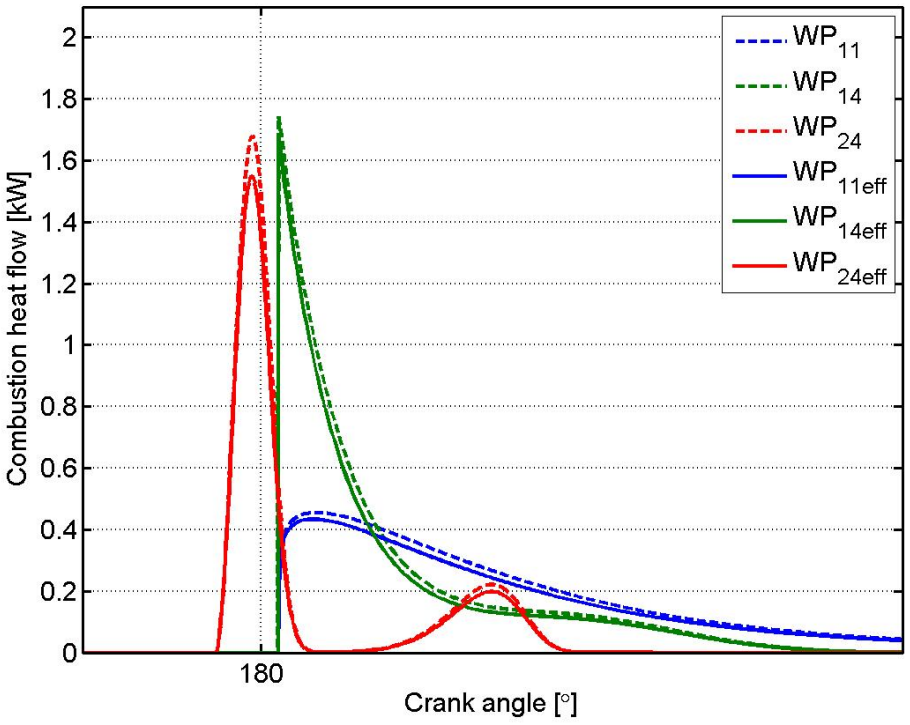

FIGURE 4.33: Instantenous combustion heat flow based on Vibe functions

4.4 Results From Vibe Functions

To illustrate the functionality of the in-cylinder process model the 3 Vibe constructed reaction rates were fed into the model and some of the outputs will be shown here.

4.4.1 Combustion Heat Flow

Using the Vibe constructed reaction rates from the smoothing attempt as input to the in-cylinder process; it is possible to calculate wanted quantities. In the figures 4.33 and 4.34 the combustion heat resulting from the Vibe constructed reaction rate is shown. The dashed lines show the combustion heat before the effect of the energy of the entering liquid fuel is added. Combustion heats follow the trend of the reaction rates and the reaction co-ordinate.

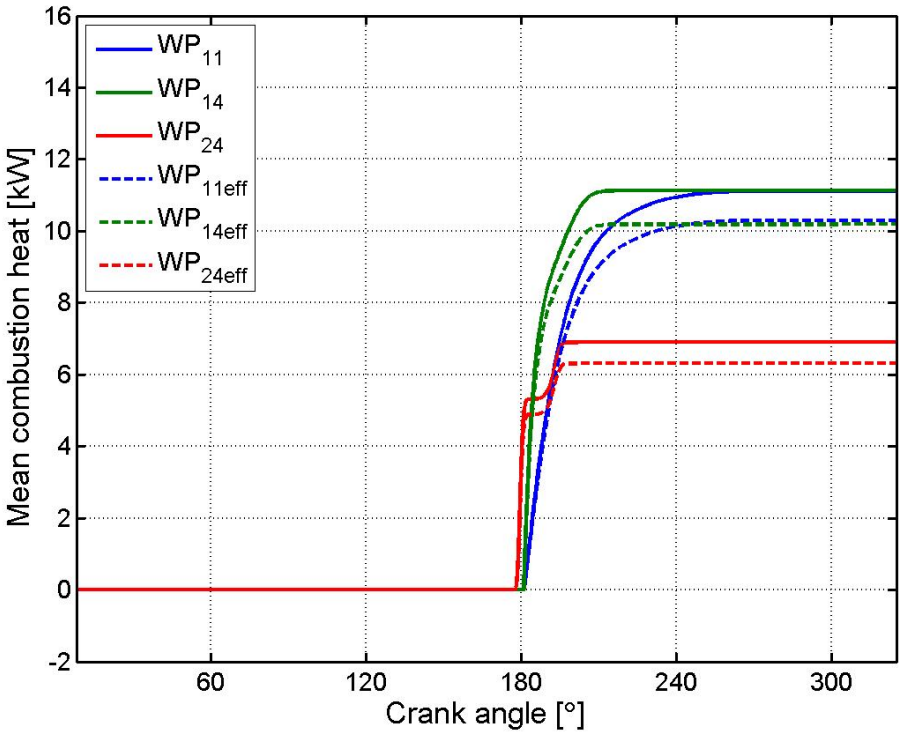

FIGURE 4.34: Mean heat flow based on Vibe functions

4.4.2 In-Cylinder Gas States

The calculated states can be seen in Figure 4.35. The figures 4.36(c) and 4.36(b), also show the states where no fuel is injected into the cylinder. In the model this means setting m_f^{comb} to zero. For WP_{24} it is easy to see the impact of the very late peak in the diffusive burning phase, which by no means is representative for the actual combustion process in the Hydra.

4.4.3 Heat Loss

Figure 4.36 shows the heat loss related quantities based on the Vibe constructed reaction rates. As for the raw data these also follow the trend of the pressure. For WP_{24} the effect of the extremely late combustion can be noticed.

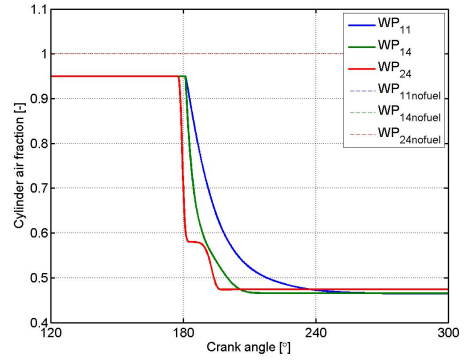

(a) Air-fraction

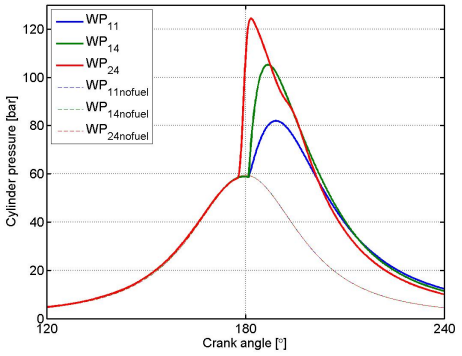

(b) Pressure

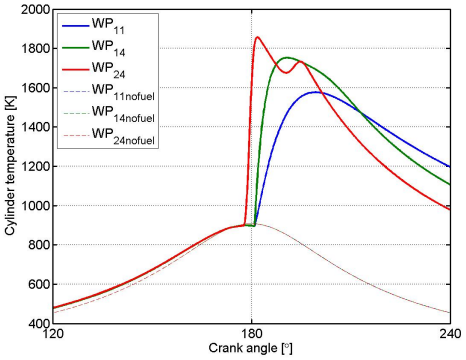

(c) Temperature

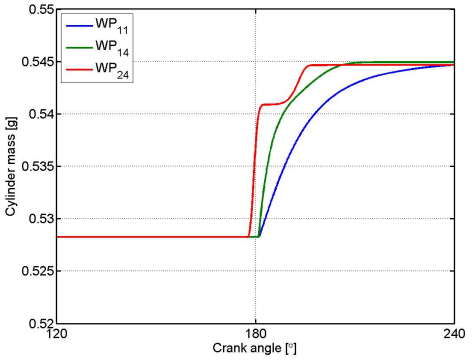

(d) Mass

FIGURE 4.35: Resulting cylinder states calculated from Vibe constructed combustion reaction rates

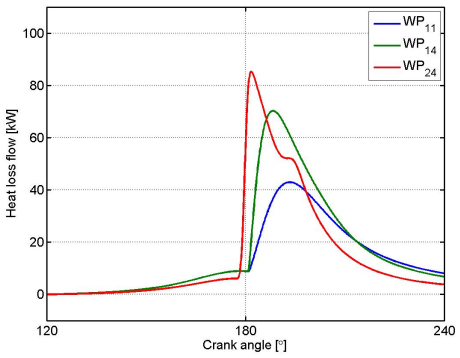

(a) Instantaneous heat loss

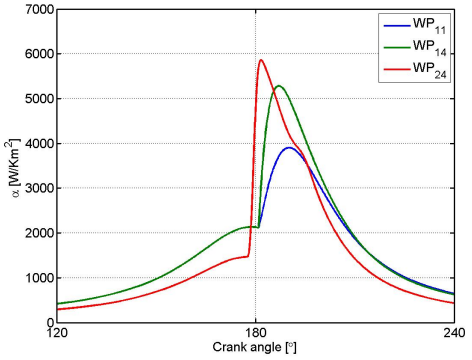

(b) Heat transfer coefficient

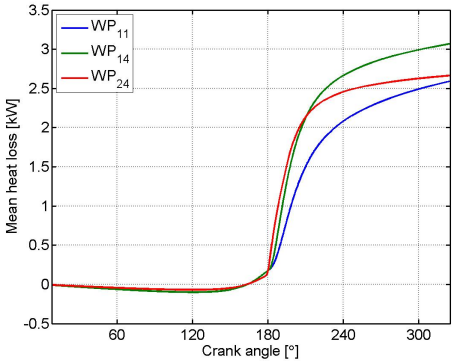

(c) Mean heat loss

4.4.4 Indicated Work

The instantaneous indicated work is shown in Figure 4.37, while the mean indicated work is shown in Figure 4.38. For WP_{11} and WP_{14} the indicated work traces are almost equal.

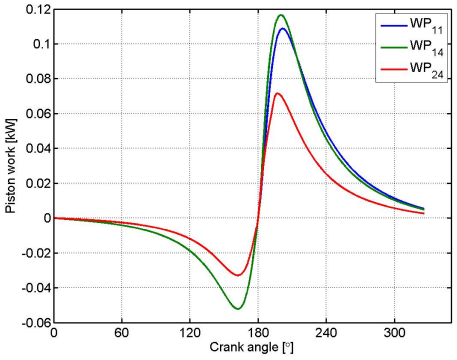

FIGURE 4.37: Instantenous indicated work

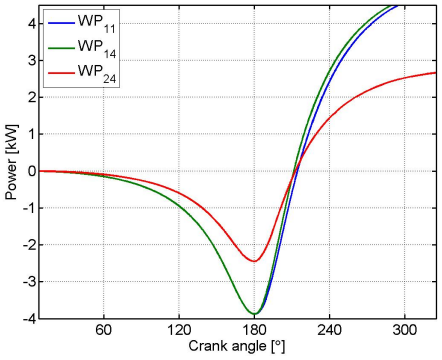

FIGURE 4.38: Mean indicated work

4.4.5 Engine Performance

The energy flows and efficiencies calculated based on the badly fitted Vibe functions becomes equally bad. For instance the indicated power is less than the actual shaft power which is impossible. This results in an efficiency that is greater than 1. The results shows that more work should be put into fitting the Vibe functions to the raw data if better more reliable results are desired.

TABLE 4.4: Caclulated engine performance based on Vibe functions

(a) Energy flow

	WP_{11}	WP_{14}	WP_{24}	
P_{shaft}	5.42	1.31	0.89	[kW]
$P_{indicated}$	4.88	4.94	2.67	[kW]
Q_{loss}	3.37	3.07	2.67	[kW]
Q_{comb}	10.15	10.19	6.30	[kW]

(b) Efficiencies

	WP_{11}	WP_{14}	WP_{24}	
η_m	1.11	0.27	0.33	[-]
η_{td}	0.72	0.69	0.73	[-]
η_{loss}	0.67	0.70	0.58	[-]
η_e	0.53	0.13	0.14	[-]

Chapter 5

Discussions

5.1 Models

An important aspect in modeling is making the program claim input from the user in such a way that wrong or illogic values are avoided. This means that some sort of control of the given input should be carried out by the program itself. The models that were made do not have a feature that checks if the given input is realistic.

In the process of constructing the models first the in-cylinder process model was built and tested on the way by using a Vibe constructed reaction rate with the example values given in chapter 2. These values were also used in Ding [2011] where the output was presented. Those presented outputs provided good aid in the verification of the output from the models presented in this thesis.

When the in-cylinder process model was made and gave satisfying results, the heat release model was constructed relatively easily by just reversing it all, so that the input was pressure instead of reaction rate. At this stage a test was done in order to check the goodness of the models. The reaction rates calculated from the raw measurements were given as input to the in-cylinder process model and

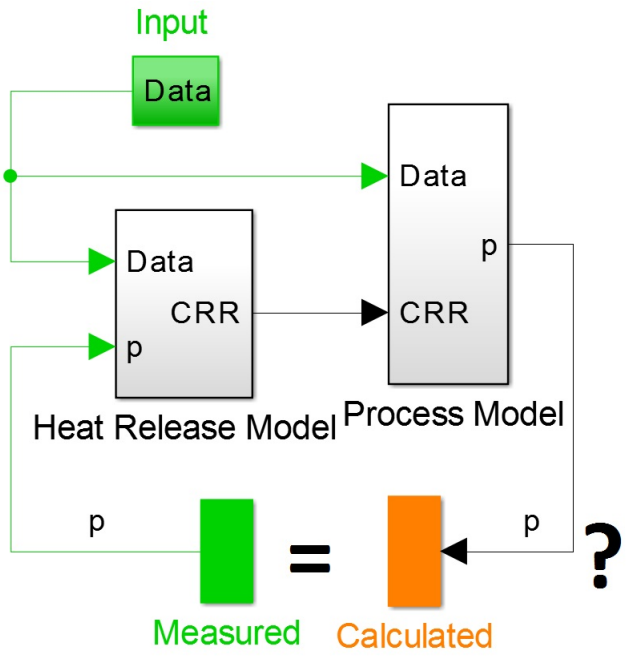

FIGURE 5.1: Concept of checking the validity of the model

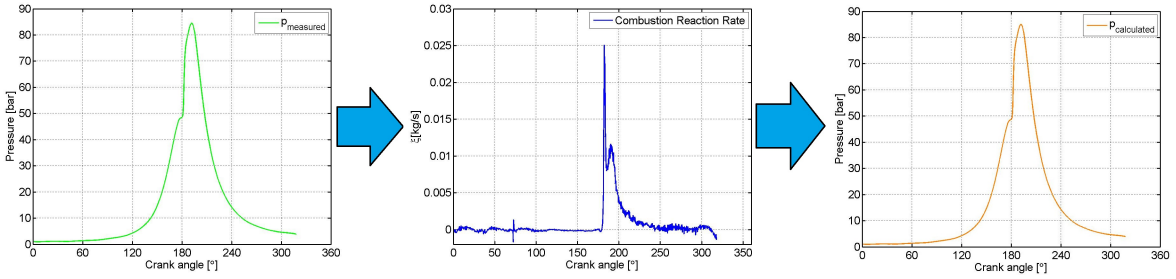

FIGURE 5.2: Raw pressure measurements and reaction rate giving new pressure WP_{11}

the calculated pressure compared to the measured. The concept is illustrated in Figure 5.1. In Figure 5.2 the measured pressure for WP_{11} giving the reaction and the resulting pressure is shown. As shown in Figure 5.3 the pressure traces are almost equal but the calculated pressure is around 0.5 [bar] higher at the peak. At the start of combustion there is a difference of about 0.25 [bar]. This could be the reason for the previously discussed impossible reaction co-ordinate.

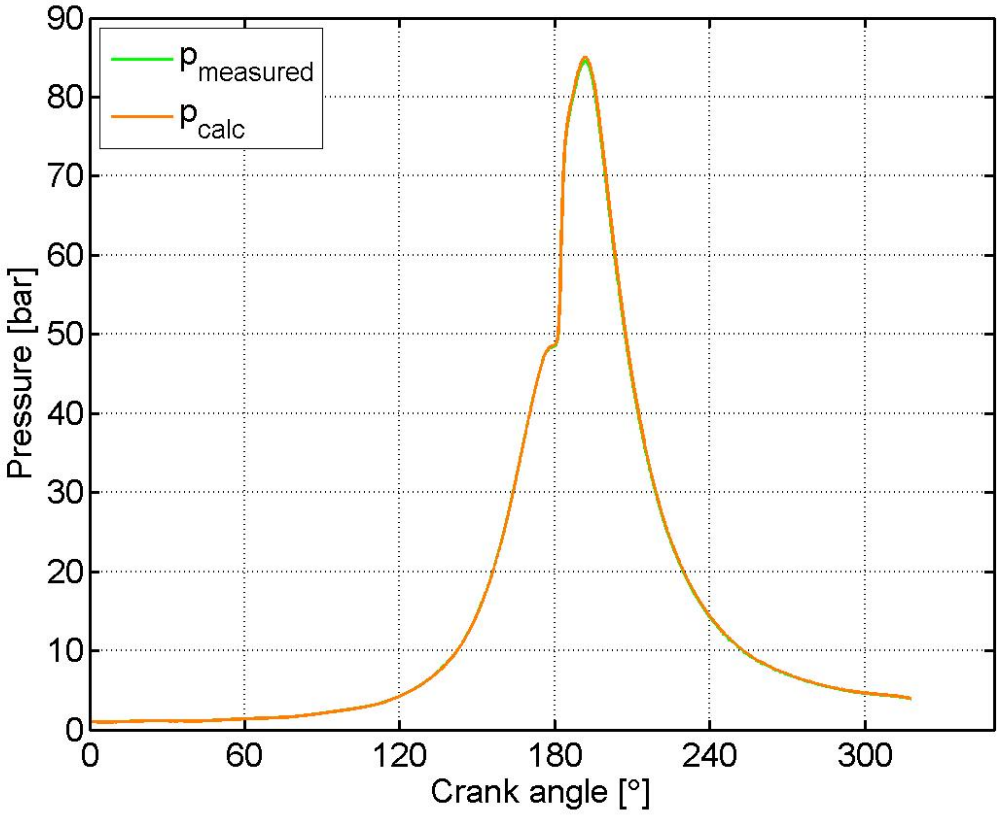

(a) Overall pressure traces

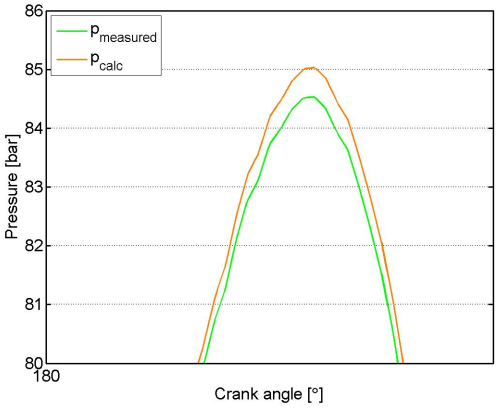

(b) Pressure peak zoom

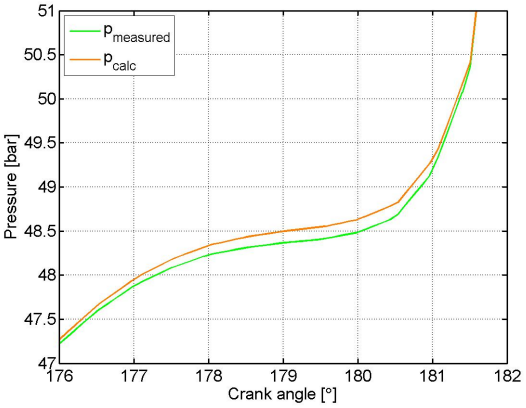

(c) Start of combustion zoom

FIGURE 5.3: Comparison of measured pressure and pressure calculated from reaction rate

5.2 Impossible Results

The reaction co-ordinate calculated from the raw pressure measurements gives a dip before the SOC, this is not possible and there may be several reasons. If the measured pressure is shifted in the negative direction this makes the RCO seem somewhat more physically correct, but it is difficult to say if this is the reason for the impossible RCO before SOC.

Changing the heat transfer coefficient obviously makes the heat loss change, but it does not seem to have that big of an impact on the RCO.

The way of measuring the crank angle has also been a matter of discussion, and shifting the crank angle gives some changes but also in this case it is hard to say something distinct about the impact on the RCO.

Changing the compression ratio makes the dip in the RCO bend upwards when ε is decreased, but these are small changes.

5.3 Smoothing

The attempt on smoothing the calculated RCO by the use of Vibe functions should be a suitable method for getting a good cylinder pressure trace. However, the experience in using the MATLAB curve fitting toolbox was non-existing and more time should have been available to get good fits. This way it would have been possible to select better start values. The engine performance calculated from the Vibe constructed reaction rate proves that the smoothing attempt is indeed poor.

5.4 Vibe vs Raw

Since the smoothing attempt gave relatively bad results, the results from the raw measurements are considered to be a lot better. Decreasing the step size in the simulation model gives already a smoothing effect on the measured pressure. In addition the integration of the reaction rate has a smoothing effect itself, and thus the further calculated results are good.

Chapter 6

Concluding Remarks

6.1 Models

The models have good functionality and can be used for different engines sizes and engine speeds. Checking the validity of the models by reversed calculation indicates this. For a more smoothed reaction rate and combustion heat flow trace it is necessary to fit the RCO with Vibe functions. This can be done by using a curve fitting toolbox which calculates the Vibe parameters.

6.2 Output

Calculation of combustion heat, heat loss, indicated work, in-cylinder states and in-cylinder thermodynamic properties with this model from raw pressure measurements on the Hydra diesel test engine gave good results. Some unrealistic values occur for the reaction co-ordinate, and the reasons for this were sought. Changing respectively the measured pressure, measured crank angle, heat transfer coefficient and geometric compression ratio gave reasons to believe that a wrongly measured pressure perhaps is causing this.

The calculated performance and efficiencies from raw pressure measurements of

the Hydra test engine shows reasonable results for the 8 different working points. For the calculated performance based on Vibe functions the results are poor. Decreasing the step size in the simulation model gives better results at this moment.

6.3 Future Work

More work should be put into fitting Vibe functions to the raw calculated RCO, such that a smooth trace of the reaction rate and thus combustion heat flow can be obtained. Better estimation of the heat transfer coefficient is possible and this can be explored and tested on the model to see if the impossible output of the reaction co-ordinate is affected. With regard to this it would also have been interesting to see if changing the swirl velocity has some sort of impact. Other types of fuel can be investigated. Considerations of the in-cylinder process by aid of the models with respect to emissions are also an interesting case, since this could not be done this time. The models can be made more user friendly.

Appendix A

Derivation Of Equation (2.1)

The derivation of (2.1) will here be presented as given in Ding [2011]. For an open control volume the energy and mass balance is shown in (A.1) and (A.2).

$$d(m \cdot u) = h^{in} \cdot dm^{in} - h^{out} \cdot dm^{out} + \delta Q - \delta W \tag{A.1}$$

$$dm = dm^{in} - dm^{out} \tag{A.2}$$

Division by time difference give energy and mass flows as shown in (A.3) and (A.4).

$$\frac{d(m \cdot u)}{dt} = h^{in} \cdot \dot{m}^{in} - h^{out} \cdot \dot{m}^{out} + \dot{Q} - \dot{W} \tag{A.3}$$

$$\frac{dm}{dt} = \dot{m}^{in} - \dot{m}^{out} \tag{A.4}$$

With no mass flow out of the control volume and the mass inflow being liquid fuel (A.3) and (A.4) can be expressed as shown in (A.5) and (A.6).

$$\frac{d(m \cdot u)}{dt} = h^{in}_{f,liq} \cdot \dot{m}^{in}_{f,liq} + \dot{Q} - \dot{W} \tag{A.5}$$

$$\frac{dm}{dt} = \dot{m}^{in}_{f,liq} \tag{A.6}$$

The total mass in the control volume is the sum of fuel mass, air mass and stoichiometric gas. Likewise the total internal energy is the sum of fuel, air and

stoichiometric internal energies. Thus the first law can be written as shown in (A.7).

$$\frac{d(m_f \cdot u_f + m_a \cdot u_a + m_{sg} \cdot u_{sg})}{dt} = h^{in}_{f,liq} \cdot \dot{m}^{in}_{f,liq} + \dot{Q} - \dot{W} \tag{A.7}$$

Differentiation of (A.7) gives (A.8).

$$m_f \cdot \frac{du_f}{dt} + m_a \cdot \frac{du_a}{dt} + m_{sg} \cdot \frac{du_{sg}}{dt} = h^{in}_{f,liq} \cdot \dot{m}^{in}_{f,liq} - u_f \cdot \frac{dm_f}{dt} - u_a \cdot \frac{dm_a}{dt} - u_{sg} \cdot \frac{dm_{sg}}{dt} + \dot{Q} - \dot{W} \tag{A.8}$$

When the dwelling time of the fuel is assumed zero and the gas assumed to behave as an ideal gas the energy balance can be expressed as shown in (A.9).

$$m \cdot C_v \frac{dT}{dt} = h^{in}_{f,liq} \cdot \dot{m}^{in}_{f,liq} - u_f \cdot \frac{dm_f}{dt} - u_a \cdot \frac{dm_a}{dt} - u_{sg} \cdot \frac{dm_{sg}}{dt} + \dot{Q} - \dot{W} \tag{A.9}$$

The 3 respective masses of substance will change when combustion takes place, and the amount that increase or decrease because of this is governed by the term $\dot{m}^{comb}_j$, such that the each mass balance can be written as shown in (A.10)- (A.12).

$$\frac{m_f}{dt} = \dot{m}^{in}_{f,gas} - \dot{m}^{comb}_f \tag{A.10}$$

$$\frac{m_a}{dt} = -\dot{m}^{comb}_f \tag{A.11}$$

$$\frac{m_{sg}}{dt} = \dot{m}^{comb}_{sg} \tag{A.12}$$

The reaction mass balance of fuel and air becoming stoichiometric gas is shown in (A.13).

$$\dot{m}^{comb}_f + \dot{m}^{comb}_a = \dot{m}^{comb}_{sg} \tag{A.13}$$

Implementing the stoichiometric ratio give (A.14) and (A.15).

$$\dot{m}^{comb}_a = \dot{m}^{comb}_f \cdot \sigma \tag{A.14}$$

$$\dot{m}^{comb}_{sg} = \dot{m}^{comb}_f \cdot (\sigma + 1) \tag{A.15}$$

Defining the reaction rate ξ as the combustion rate $\dot{m}_f^{comb}$, and substituting into (A.10) - (A.12) give (A.16) - (A.18).

$$\frac{m_f}{dt} = \dot{m}_{f,gas}^{in} - \xi \tag{A.16}$$

$$\frac{m_a}{dt} = -\sigma \cdot \xi \tag{A.17}$$

$$\frac{m_{sg}}{dt} = (1+\sigma) \cdot \xi \tag{A.18}$$

The energy balance can now be written as shown in (A.19).

$$m \cdot C_v \frac{dT}{dt} = h_{f,liq}^{in} \cdot \dot{m}_{f,liq}^{in} - u_f \cdot (\dot{m}_{f,gas}^{in} - \xi) + u_a \cdot \sigma \cdot \xi - u_{sg} \cdot (1+\sigma) \cdot \xi + \dot{Q} - \dot{W} \tag{A.19}$$

The inflow of fuel mass will be equal to the mass flow of fuel evaporating as gas from the fuel droplets. Then (A.19) can be sorted and expressed as shown in (A.20).

$$m \cdot C_v \frac{dT}{dt} = \dot{m}_f^{in} \cdot (h_{f,liq}^{in} - u_f) + \xi \left[(u_f + \sigma \cdot u_a - (1+\sigma) \cdot u_{sg}) \right] + \dot{Q} - \dot{W} \tag{A.20}$$

Introducing the combustion heat flow as shown in (A.21), and the negative effect of transporting liquid fuel into the cylinder as shown in (A.22).

$$\dot{Q}_{comb} = \xi \left[(u_f + \sigma \cdot u_a - (1+\sigma) \cdot u_{sg}) \right] \tag{A.21}$$

$$\dot{E}_f = \dot{m}_{f,in} \cdot (h_{f,liq}^{in} \cdot -u_f) \tag{A.22}$$

With the reversible indicated work and the heat loss giving rise to negative terms in the energy balance we have (A.23).

$$m \cdot C_v \frac{dT}{dt} = \dot{Q}_{comb} - \dot{Q}_{loss} - p \cdot \frac{dV}{dt} + \dot{E}_f \tag{A.23}$$

In the end arriving at (2.1) as shown in (A.24).

$$\frac{dT}{dt} = \frac{\dot{Q}_{comb} - \dot{Q}_{loss} - p \cdot \frac{dV}{dt} + \dot{E}_f}{m \cdot C_v} \tag{A.24}$$

Appendix B

Thermodynamical Properties

TABLE B.1: Power series coefficients [Stapersma, 2010c],[Ding, 2011]

	a_1	a_2	a_3	a_4	a_5	a_6	range [K]
N_2	3.5463	-0.5773	1.8224	-1.1149	0.2731	-0.0239	200-2500
O_2	3.0845	1.8622	-1.0049	0.2817	-0.0320	0.0007	200-2500
Ar	2.5000	0	0	0	0	0	200-2500
CO_2	2.5468	8.0614	5.9398	2.2908	-0.4380	0.0327	200-2500
H_2O	3.9800	-0.4380	2.5797	-1.4469	0.3244	-0.0264	200-2500
SO_2	3.5220	0.0660	1.0660	-0.7510	0.1930	-0.0170	200-2500
$C_{13}H_{10}$ (gas)	-74.758	1018.7	-717.21	221.40	-20.280	0	200-1500
$C_{13}H_{28}$ (gas)	110.40	533.21	739.84	-1021.2	324.23	0	150-1500
$C_{13}H_{10}$ (liquid)	2210	0	0	0	0	0	-
$C_{13}H_{28}$ (liquid)	1700	0	0	0	0	0	-

TABLE B.2: Reference enthalpies for species in cylinder gas, p=100 [kPa] and T=25 °C[Ding, 2011]

Species	h_{ref} [kJ/kg]
N_2	0
O_2	0
Ar	0
CO_2	-8941.4
H_2O	-1342.3
SO_2	-9890.7

TABLE B.3: Reference evaporation enthalpies for aromat and alkene, p=100 [kPa] and T=25 °C[Ding, 2011]

Species	h_{ref}^{evap} [kJ/kg]
$C_{13}H_{10}$	339
$C_{13}H_{28}$	246

Appendix C

Effects Of Changing α, CA, p, ϵ

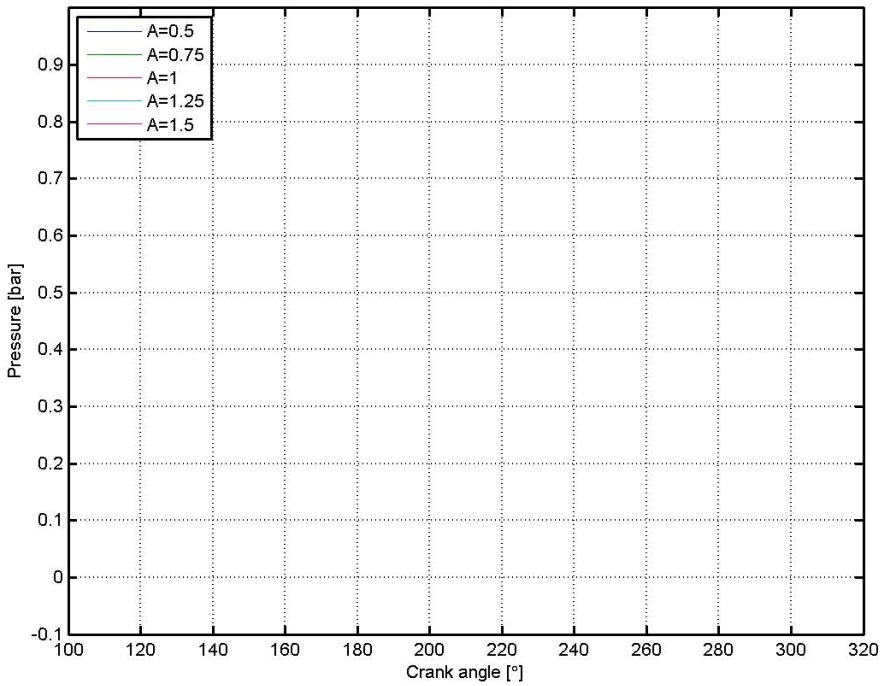

FIGURE C.1: Effect of changing the heat transfer coefficient on the cylinder pressure at WP_{11}

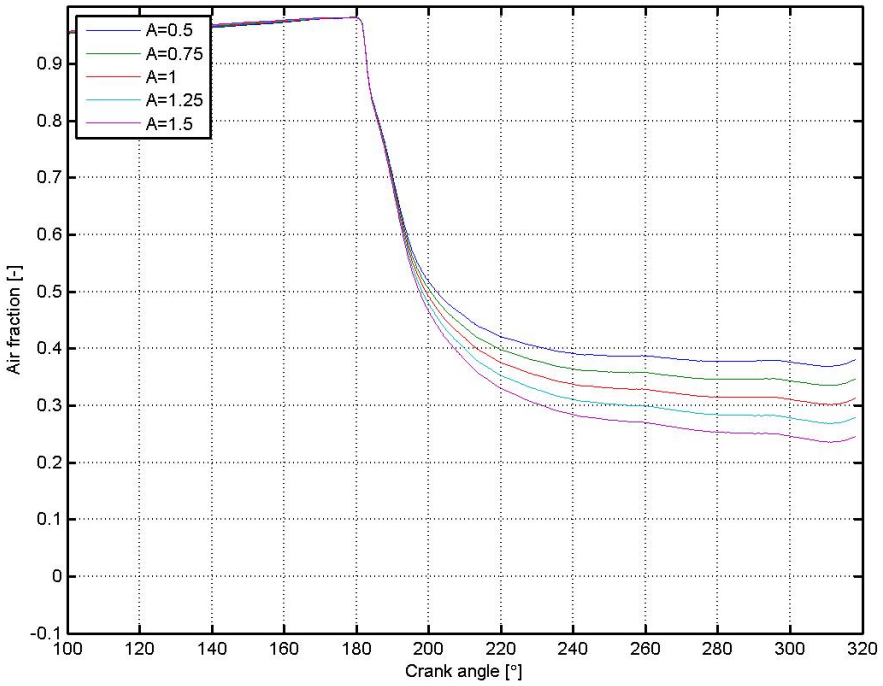

FIGURE C.2: Effect of changing the heat transfer coefficient on the in-cylinder air fraction at WP_{11}

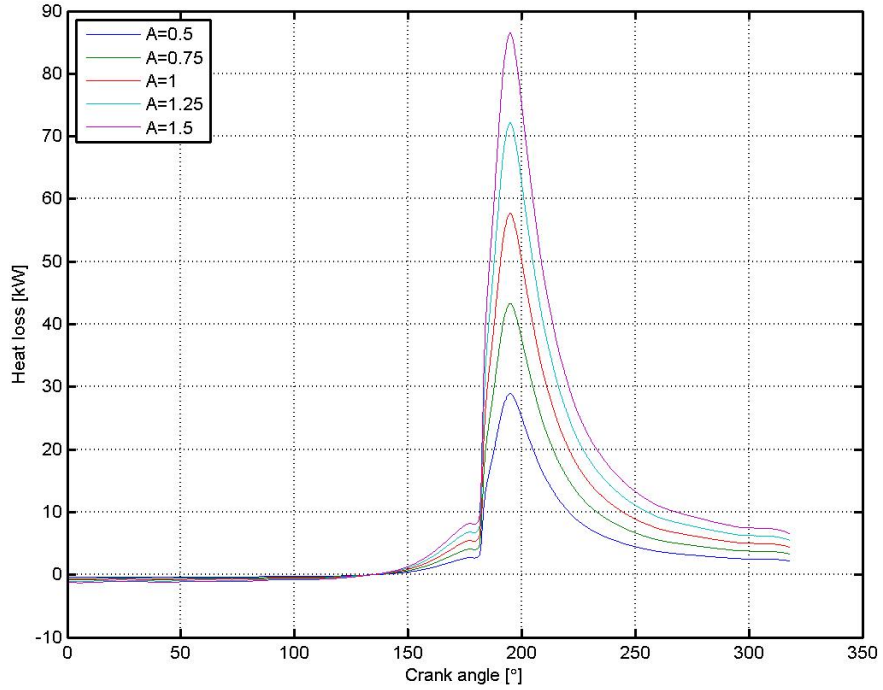

FIGURE C.3: Effect of changing the heat transfer coefficient on the heat loss at WP_{11}

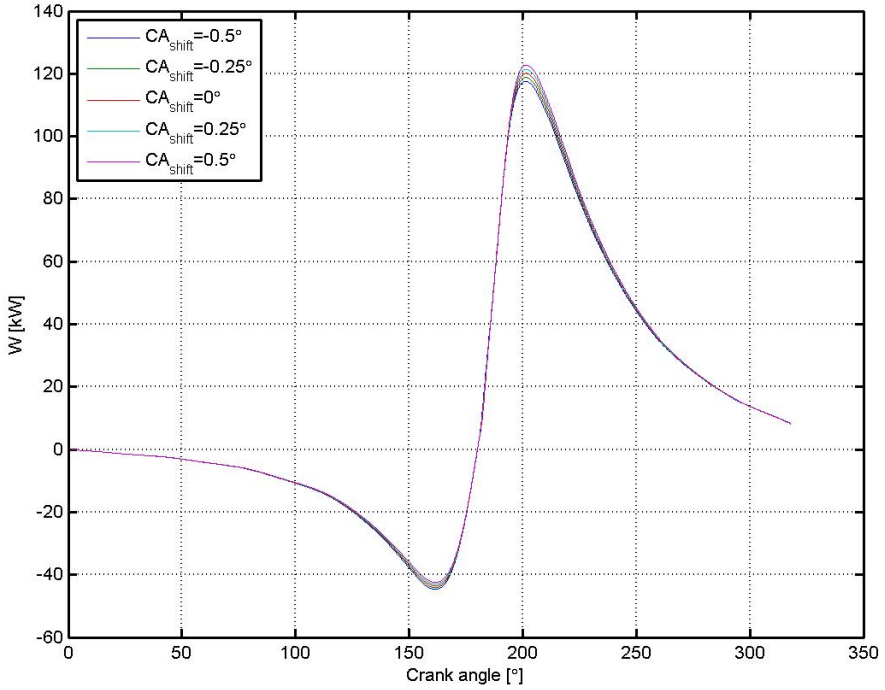

FIGURE C.4: Effect of changing the heat transfer coefficient on the indicated work at WP_{11}

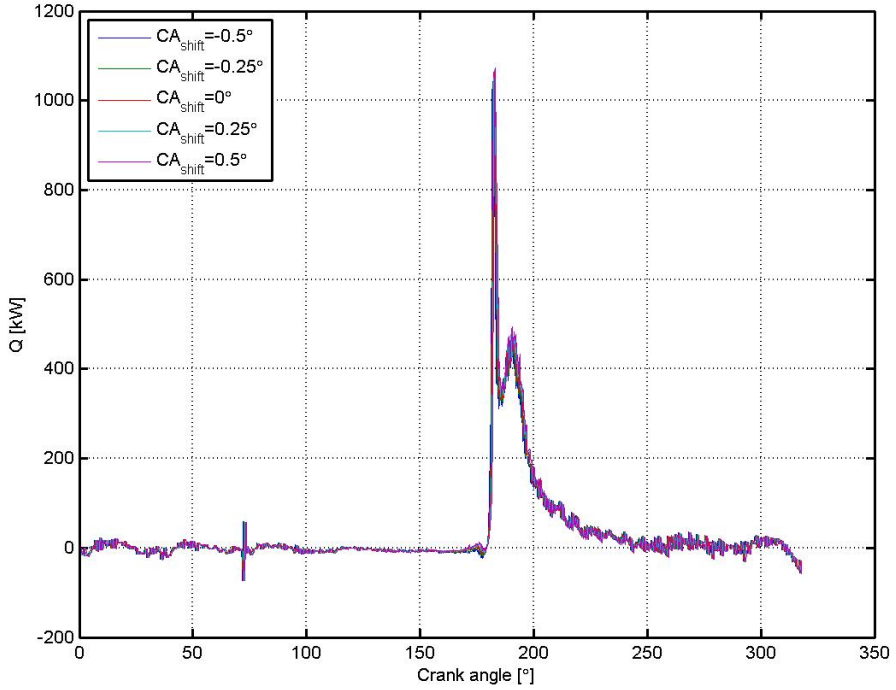

FIGURE C.5: Effect of changing the heat transfer coefficient on the combustion heat flow at WP_{11}

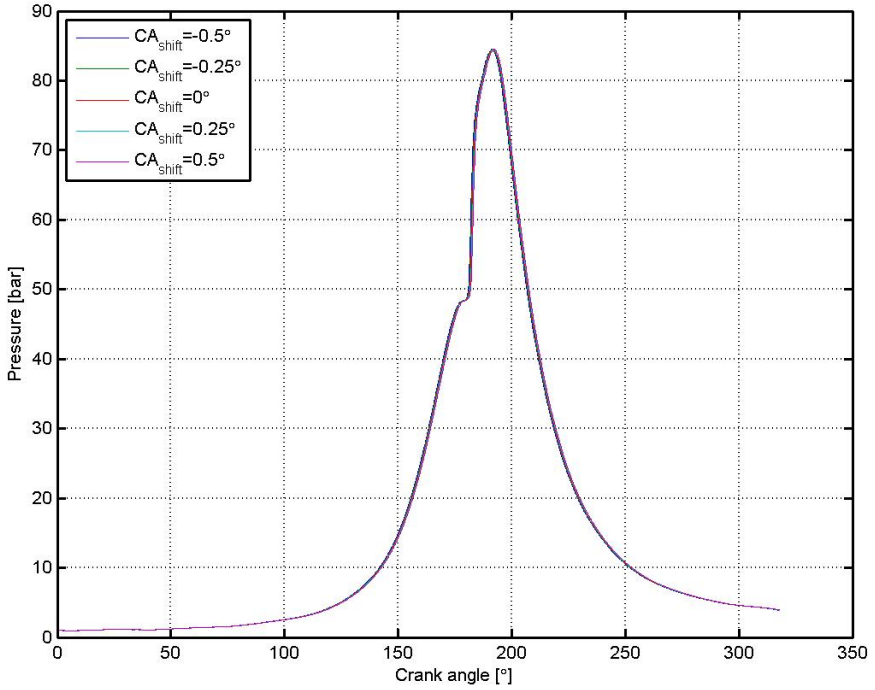

FIGURE C.6: Effect of shifting the measured crank angle on the cylinder pressure at WP_{11}

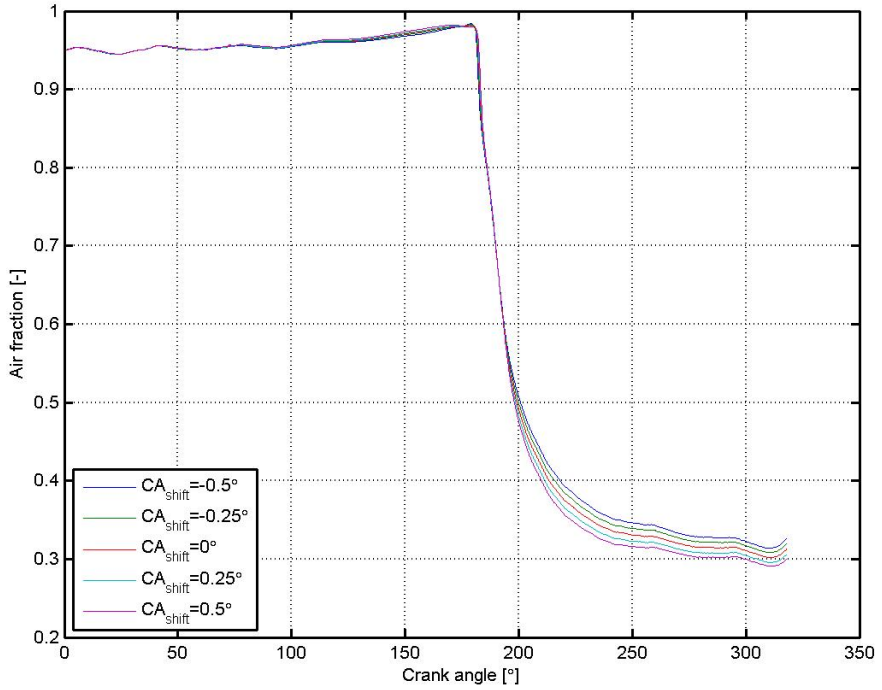

FIGURE C.7: Effect of shifting the measured crank angle on the in-cylinder air fraction at WP_{11}

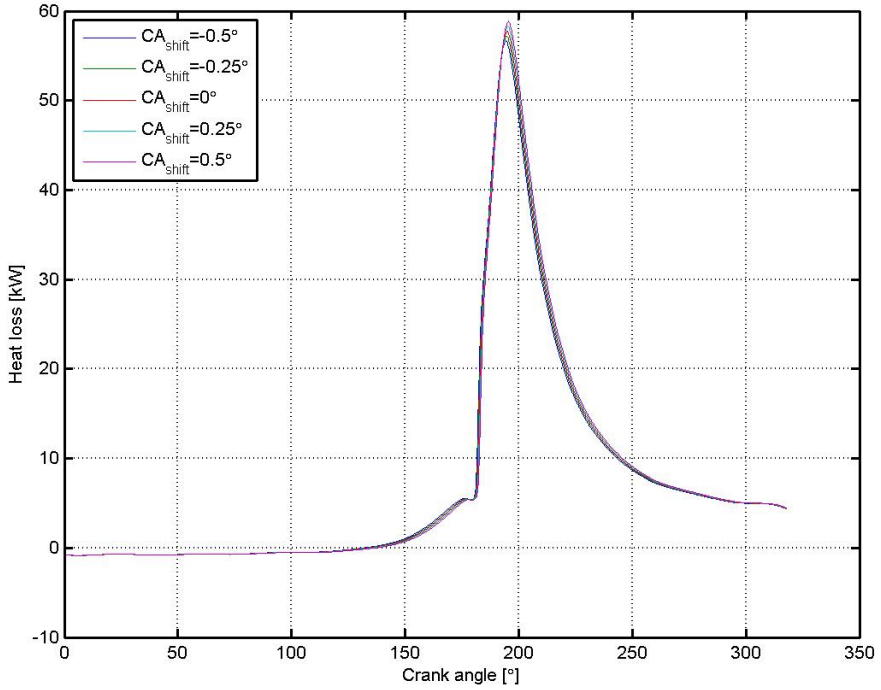

FIGURE C.8: Effect of shifting the measured crank angle on the heat loss WP_{11}

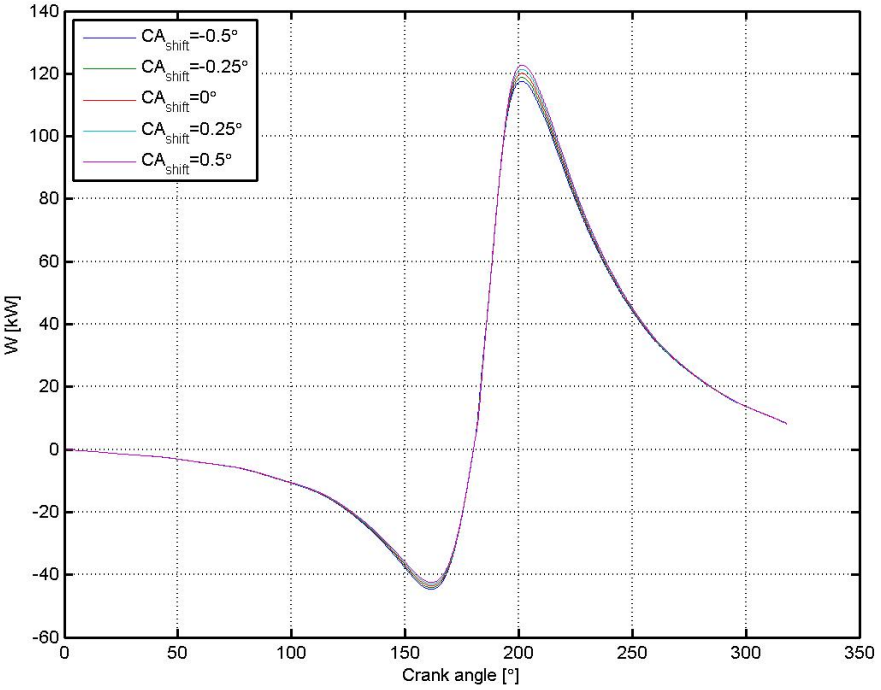

FIGURE C.9: Effect of changing the measured crank angle on the indicated work at WP_{11}

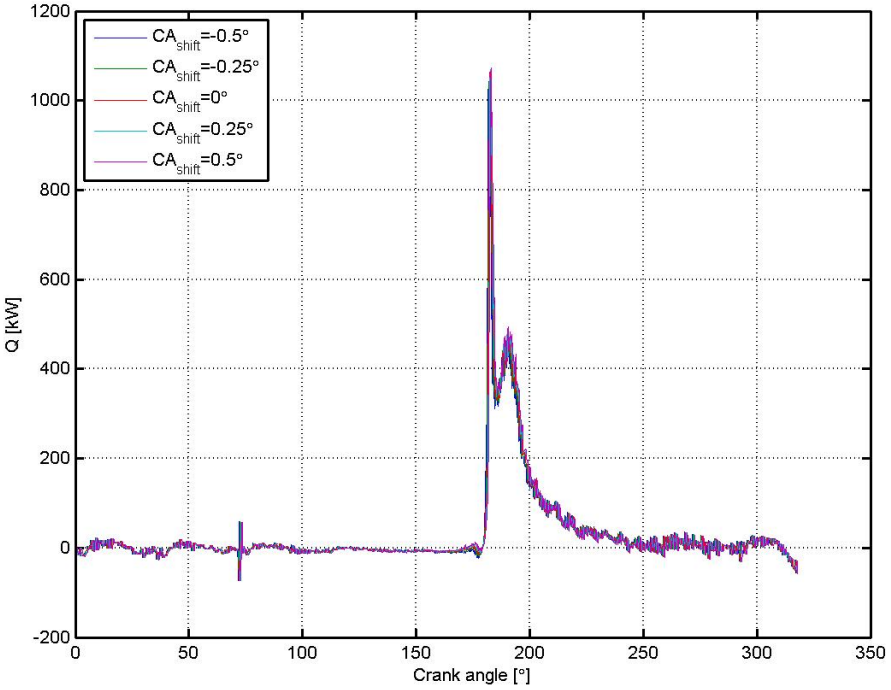

FIGURE C.10: Effect of changing the measured crank angle on the combustion heat flow at WP_{11}

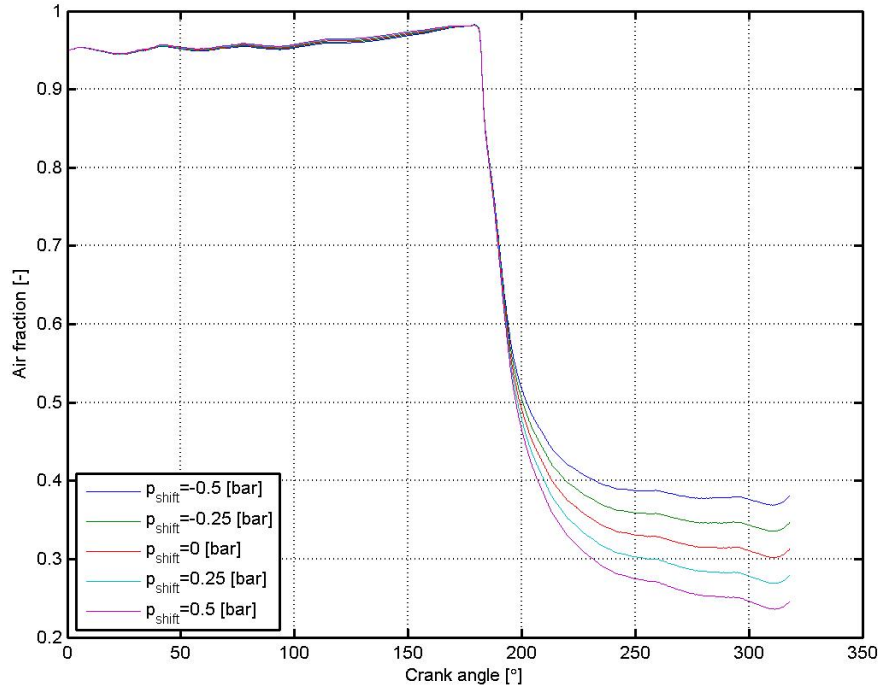

FIGURE C.11: Effect of shfiting the measured pressure on the in-cylinder air fraction at WP_{11}

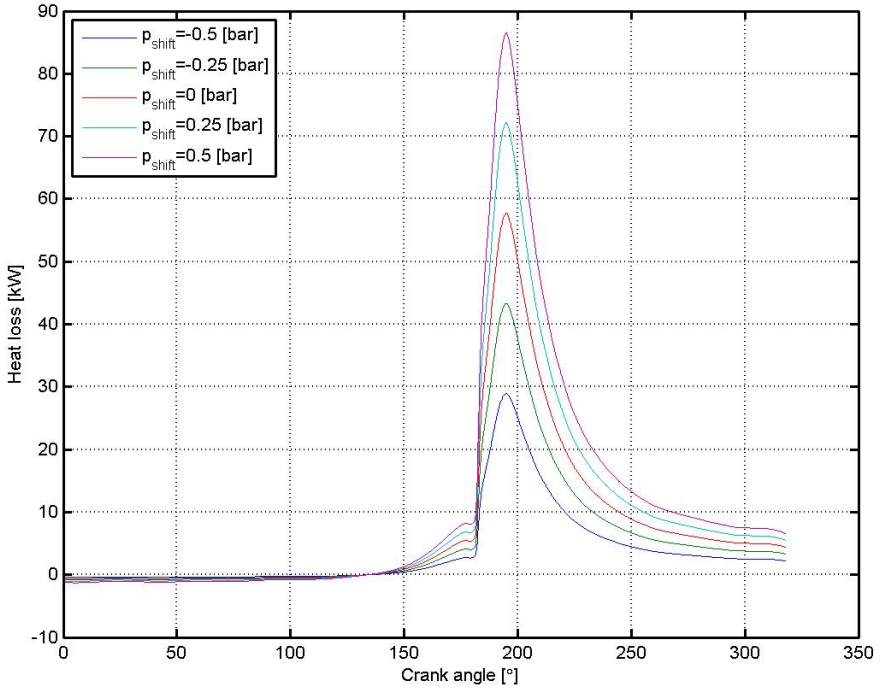

FIGURE C.12: Effect of changing the measured pressure on the heat loss at WP_{11}

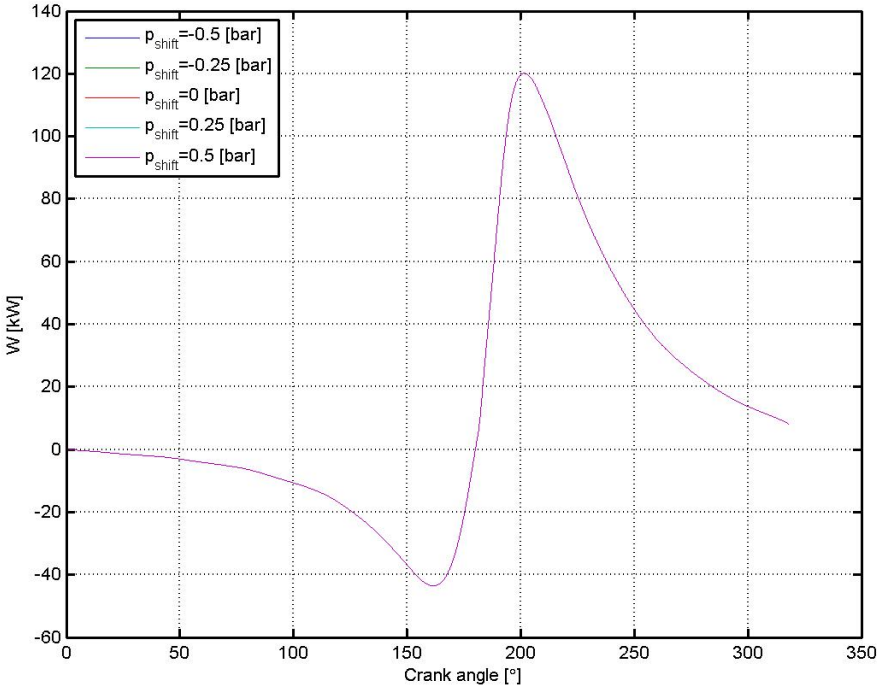

FIGURE C.13: Effect of changing the measured pressure on the indicated work at WP_{11}

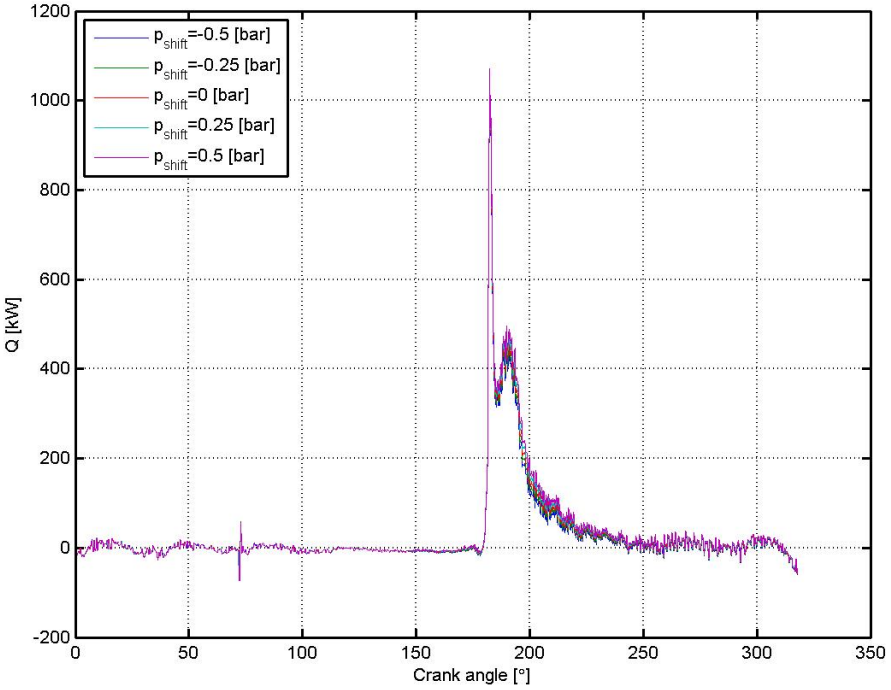

FIGURE C.14: Effect of changing the measured pressure on the combustion heat flow at WP_{11}

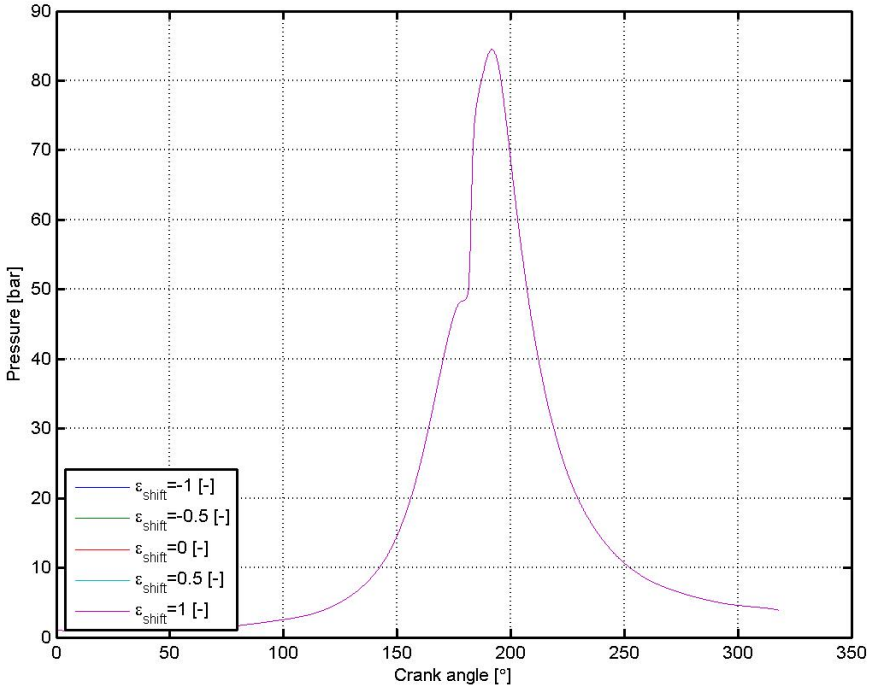

FIGURE C.15: Effect of changing the measured pressure on the cylinder pressure at WP_{11}

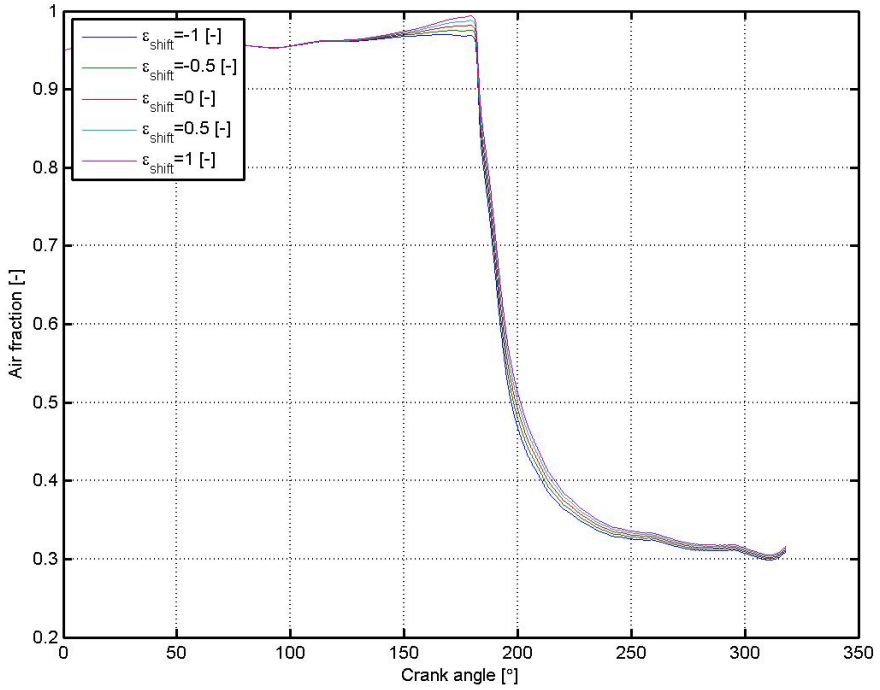

FIGURE C.16: Effect of shfiting the measured pressure on the in-cylinder air fraction at WP_{11}

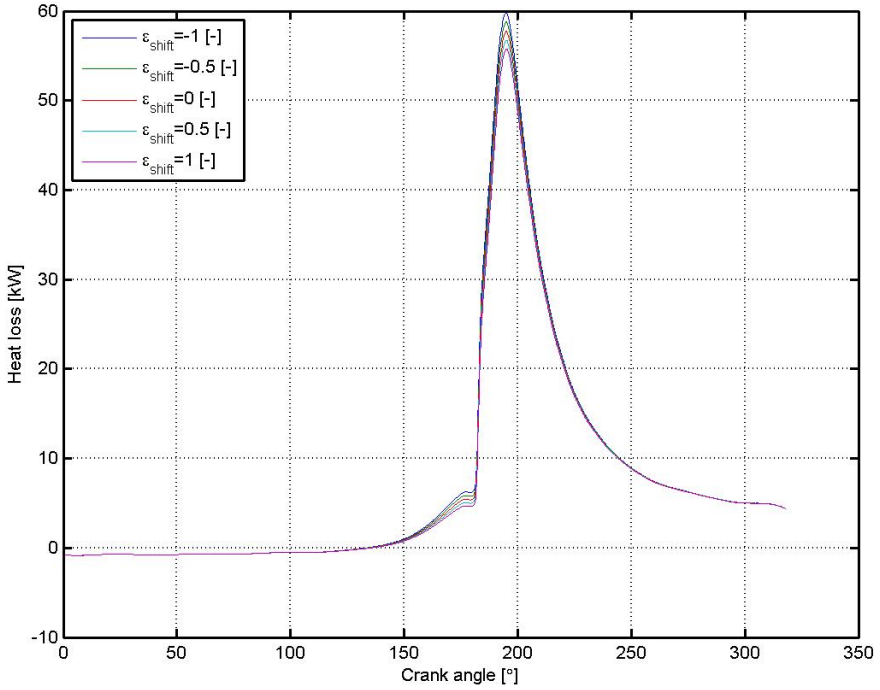

FIGURE C.17: Effect of changing the measured pressure on the heat loss at WP_{11}

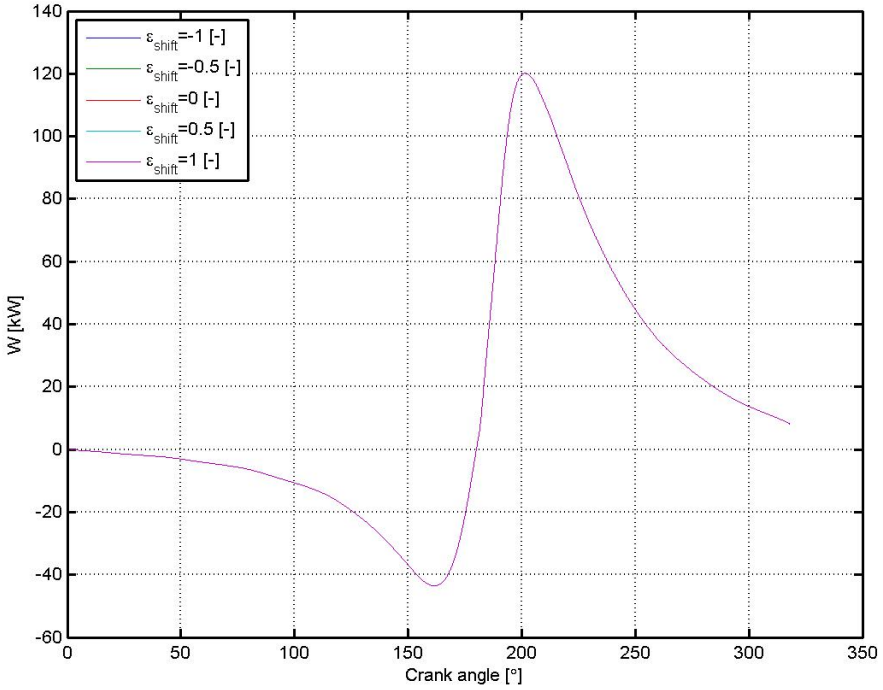

FIGURE C.18: Effect of changing the compression ratio on the indicated work at WP_{11}

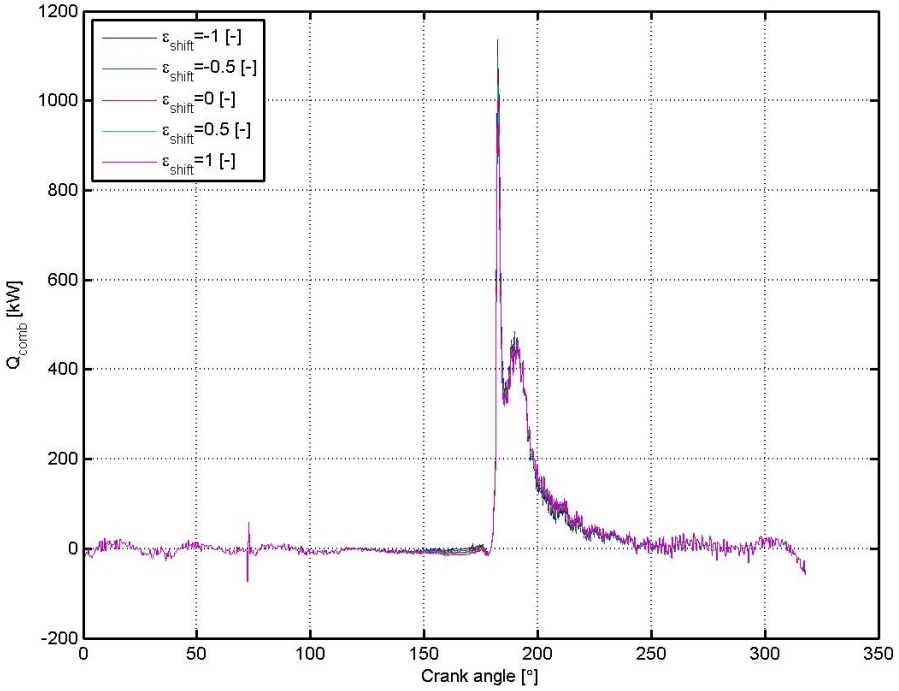

FIGURE C.19: Effect of changing the compression ratio on the combustion heat flow at WP_{11}

Appendix D

Details For Use Of Simulation Models

For using the in-cylinder process model to simulate the pressure from a Vibe constructed reaction rate it is necessary to set some input values. The name of this file is "MODEL.slx". By double-clicking the green input block as shown in Chapter 3, the sub-model will be as shown in Figure D.1. The green blocks are where input must be set by the user. Opening the "Engine Dimensions" block will show the MATLAB function shown in Listing D.1, where the values can be set. Opening the "Start Conditions" block will give the MATLAB function shown in Listing D.2, and the necessary input start conditions can be set. The block "Fuel Specification" gives the MATLAB function shown in Listing D.3, and here the information of the fuel is put in. The rest of the input parameters are set by double clicking the green blocks.

For using the heat release model pressure measurements must be available with their corresponding crank angles. The pressure without fuel injection must also be available. The name of this model is "ROHRMODEL.slx". It is simple to run this model from a MATLAB script. See Listing D.4 for an example of how this can be done. Here the "Inndata.m" loads pressure measurements taken on the Hydra. The model can be run by writing "sim('ROHRMODEL',[0 (60/N)])" in

the command window. The numbers in the square brackets are the start of the simulation and the end of the simulation.

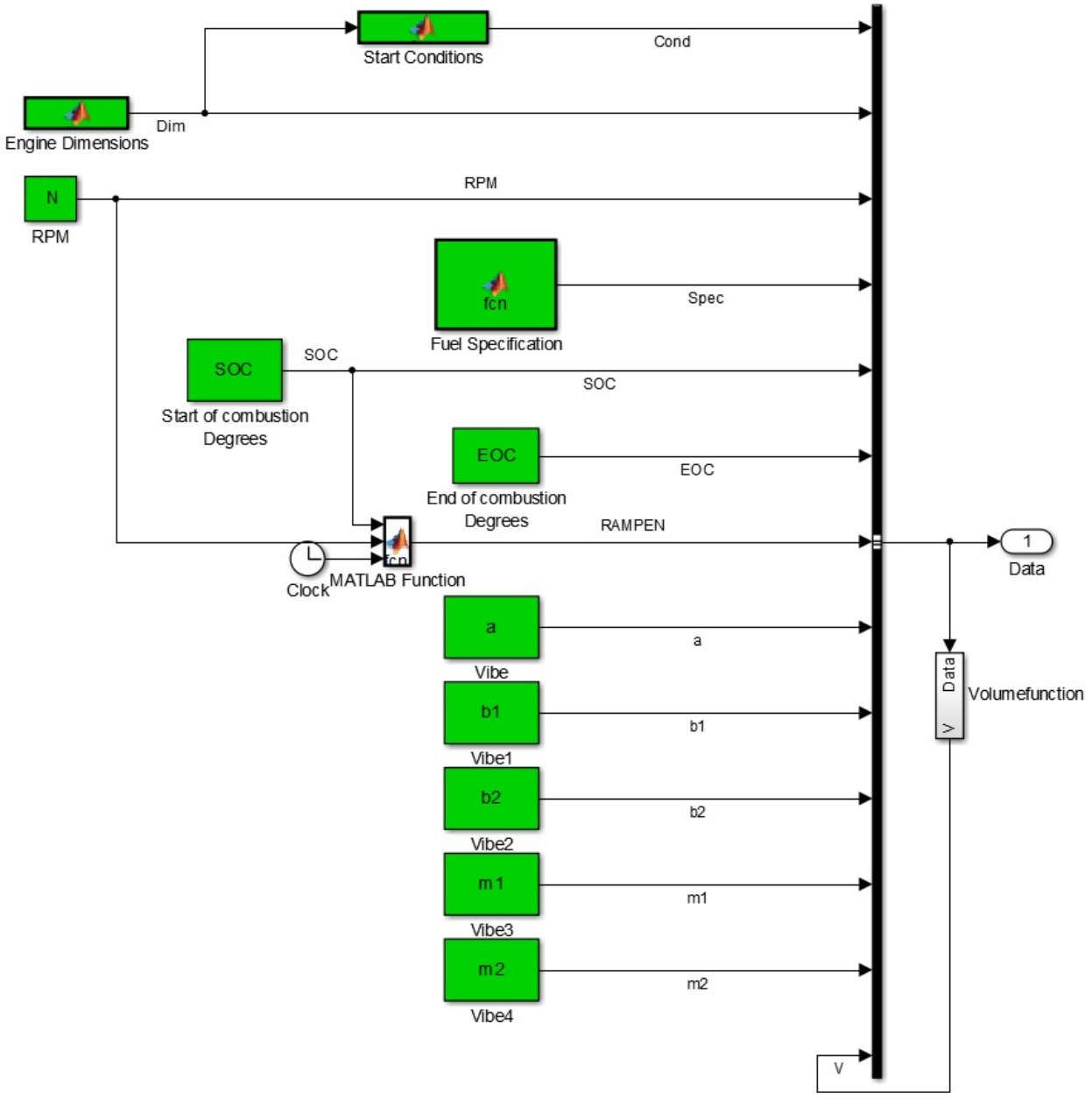

FIGURE D.1: In-cylinder process model input submodel

```
function Dim = fcn()
%#codegen
%input parameters————————————————————————
Db=0.07835; %bore diameter [m]
Ls=0.0889; %stroke length [m]
eps=19.5228; %geometric compression ratio
Lcr=0.158; %connecting rod length
%————————————————————————————————————————
Ab=(pi/4)*Db^2; %bore area [m^2]
lambdaCR=Ls/(2*Lcr); %crank/rod ratio
Dim=[Db Ab Ls eps Lcr lambdaCR];
```

LISTING D.1: Engine specification input

```
function Cond = fcn(Dim)
%#codegen
%input parameters————————————————————————
phi_IC=8; %inlet closes [degree]
x1=0.95; %air fraction at beginning
lambda=2; %air excess ratio
p1b=1.0; %trapped pressure [bar]
T1=297; %trapped temperature [K]
%————————————————————————————————————————
R1=287; %J/kgK
p1=p1b*10^5; %Pascal
a=phi_IC*(pi/180); %crank angle in radians
Db=Dim(1); %bore in m
Ab=Dim(2); %bore area m^2
Ls=Dim(3); %stroke length m
eps=Dim(4); %geometric compression ratio
Lcr=Dim(5); %connecting rod length
lambdaCR=Dim(6); %crank/rod ratio
Lp=Ls*((1/(eps-1))+0.5*((1+cos(a))+(1/lambdaCR)
*(1-sqrt(1-(lambdaCR^2)*(sin(a))^2))));
V1=Lp*Ab; %trapped volume
m1=(p1*V1)/(R1*T1);
```

```
23 Cond=[m1 x1 lambda V1 T1 p1b];
```

Listing D.2: Start conditions input

```
1  function Spec = fcn
2  %#codegen
3  %input fuel mass fractions and density at 15 degree celsius
4  x_c=0.8478; x_h=0.1495; x_s=0.00; x_ash=0; x_h2o=0;
5  rho_f_15=830;
6  %------------
7  M_c=12.0107; M_h=1.00794; M_s=32.065;
8  M_alk=13*M_c+28*M_h;
9  M_aro=13*M_c+10*M_h;
10 M_da=28.964;
11 y_O2_da=0.21;
12 sigma_da=(M_da/y_O2_da)*((x_c/M_c)+((1/4)*(x_h/M_h))+(x_s/M_s));
13 x_alk=(x_c-((13*M_c)/M_aro)*(x_c+x_h))/(((13*M_c)/M_alk)
14 -((13*M_c)/M_aro));
15 x_aro=x_c+x_h-x_alk;
16 LHVref=(46932-((8792*rho_f_15^2)/1000000)+((3187*rho_f_15)/1000))
17 *(1-x_h2o-x_ash-x_s)+(9420*x_s)-(2499*x_h2o);
18 Spec=[x_c x_h x_s sigma_da x_alk x_aro LHVref rho_f_15];
```

Listing D.3: Fuel specification input

```
1  clear;
2  %load pressure measurements
3  Inndata;
4  CAshift=0; %set crank angle shift
5  A=1; %set factor A for heat transfer coefficient
6  pshift=-0.5; %set pressure shift
7  N=18.9*60; %set engine speed
8  CA=CA24; %Crank angle for WP24
9  p=p24; %Measured pressure for WP24
10 p0=p240; %Measured pressure for WP24 without fuel injection
11 SOC=177.5; %Start of combustion
```

```
12 EOC=216; %End of combustion
```

Listing D.4: Script for running "ROHRMODEL.slx"

Bibliography

D. Stapersma. *Diesel Engines Performance Analysis*, volume 1. Delft University of Technology, 2010a.

A.E. Atabani, A.S. Silitonga, Irfan Anjum Badruddin, T.M.I. Mahlia, H.H. Masjuki, and S. Mekhilef. A comprehensive review on biodiesel as an alternative energy resource and its characteristics. *Renewable and Sustainable Energy Reviews*, 16(4):2070 – 2093, 2012. ISSN 1364-0321. doi: 10.1016/j.rser.2012.01.003. URL `http://www.sciencedirect.com/science/article/pii/S1364032112000044`.

D. Stapersma. *Diesel Engines Combustion*, volume 3. Delft University of Technology, 2010b.

Yu Ding. *Characterising Combustion in Diesel Engines*. PhD thesis, TU Delft, 2011.

D. Stapersma. *Diesel Engines - Thermodynamical Principles 2*, volume 6. Delft University of Technology, 2010c.

D. Stapersma. *Diesel Engines Emissions and Heat Transfer*, volume 4. Delft University of Technology, 2010d.

Nadine Grace Mosteiro Halvorsen. Gtl produkter som marint drivstoff. Master thesis, NTNU.